Constraining Aerosol Health Impacts with Sensitivity Analysis using the Adjoint of CMAQ

Comprehensive Exam Report

Matthew Turner[1]
Advisor: Professor Daven Henze[1]
Collaborators: Hakami, A.[2]; Zhao, S.[2]; Resler, J.[3]; Carmichael, G.[4]; Stanier, C.[4]; Baek, J.[4]; Saide, P.[4]; Sandu, A.[5]; Russel, A.[6]; Jeong, G.[6]; Nenes, A.[6]; Capps, S.[8]; Percell, P.[7]; Pinder, R.[8];Napelenok, S.[8]; Pye, H.[8]; Bash, J.[8]; Chai, T.[9]; Byun, D.[9]

[1] *University of Colorado at Boulder*
[2] *Carleton University*
[3] *ICS Prague*
[4] *University of Iowa*
[5] *Virginia Tech*
[6] *Georgia Tech*
[7] *University of Houston*
[8] *USEPA*
[9] *NOAA*

January, 2014

Contents

1 Abstract

Long-term exposure to fine particulate matter is associated with adverse health effects such as premature mortality, ischemic heart disease, and congestive heart failure. In 2011, the World Health Organization estimated that urban outdoor air pollution is the cause of approximately 1.3 million premature deaths worldwide per year. Of these, the U.S. EPA estimates that 141,000 cardiopulmonary and lung cancer deaths are due to exposure to fine particulate matter ($PM_{2.5}$) in North America. Studies have suggested that $PM_{2.5}$ mixtures with a high concentration of BC may have greater effects on mortality than mixtures low in BC. Quantifying the role of emissions from different sectors and different locations in governing the total health impacts is critical towards developing effective control strategies. To answer such questions, an adjoint model can provide sensitivities of excess mortality (through the use of the concentration response functions) with respect to emissions at a highly resolved spatial and sectoral level of specificity. As such, the current Community Multiscale Air Quality (CMAQ) adjoint model has been updated to include aerosols.

In this work, we use the CMAQ adjoint model to quantify the role of emissions from different sectors and different locations on premature mortalities attributed to exposure to BC. The adjoint model is first validated by comparing adjoint sensitivities to both finite difference and complex variable sensitivities. A majority of mortalities attributed to exposure to BC occur in highly populated areas. Here, we are able to show for the first time the fraction of the mortality owning to transport from less populated regions. The results suggest that placing emissions regulations on the locations with highest emission would not necessarily be the most effective strategy to reduce mortalities attributed to BC exposure. Several areas upwind of highly populated areas have a much higher contribution to mortality than local incidence of mortality itself.

2 Motivation and Objectives

Particulate Matter (PM) is an air pollutant consisting of a mixture of solid and liquid particles suspended in the air. Knowledge of the sources and distributions of PM is important for many reasons, two of which are that PM has an adverse effect on human health (Amann et al., 2006; Lepeule et al., 2012), and PM also has an effect on climate change. Since its inception in 1970, the U.S. Environmental Protection Agency (EPA) has been tasked with the protection of human health and the environment. Title I of the Clean Air Act dictates that the EPA is in charge of setting National Ambient Air Quality Standards (NAAQS) for air pollutants that may endanger public health or welfare. In addition to the development of NAAQS, the EPA evaluates the cost and effectiveness of emissions control policies and monitors NAAQS exceedences. One major aspect of this process is the use of air quality models to estimate current and future distributions of fine particulate matter ($PM_{2.5}$).

Many atmospheric chemical transport models (CTM) can simulate the distribution and fate of aerosols. However, many of these models contain considerable uncertainty. There are several different methods to decrease uncertainty in the models, such as developing a better understanding of the physical processes, using data assimilation techniques to constrain the

models with observations, and using an ensemble of models to obtain robust results. These approaches allow us to make use of air quality models for understanding source-receptor relationships. Quantifying the role of emissions from different sectors and different locations in governing the total health impacts is critical towards developing effective control strategies.

This project focuses on reducing uncertainty in sources of aerosols that have an adverse human health impact through the development and application of adjoint modeling for sensitivity and inverse studies. This thesis will address the following research objectives:

1. Develop the adjoint of aerosol microphysics for the CMAQ adjoint model.
2. Use adjoint sensitivity analysis to attribute health impacts to emissions from specific locations, species, and sectors to facilitate more effective air quality control strategies.
3. Accurately estimate regional radiative and air quality impacts of aerosols, by constraining emissions through the use of inverse modeling.

This project will result in the first air quality adjoint that includes an adjoint of aerosol size distribution, improving the overall applicability of the CMAQ model. Accounting for the particle size distribution is important for both health and climate concerns, as it is associated with the particle origin, their transport in the atmosphere, and the degree to which they are inhaled into the respiratory system (Amann et al., 2006).

This project begins with the development of an adjoint model, which is necessary for the 4D-Variational data assimilation technique, of the CMAQ chemical transport model. In addition to the ability to use an adjoint model for data assimilation, adjoint models provide an efficient means of performing sensitivity analysis. As opposed to forward sensitivity techniques, where sensitivities of all state variables with respect to a few parameters (inputs) are calculated, adjoint sensitivity analysis calculates the sensitivity of a single model response metric with respect to all sources (Giering and Kaminski, 1998). For example, an adjoint model can provide sensitivities of excess mortality (through the use of the concentration response functions) with respect to emissions at a highly resolved spatial and sectoral level. This tool can be used to determine the sensitivity of mortality in a region with respect to emissions throughout the modeled domain.

Here we present the background, initial application, and future directions for this thesis. Section 3 reviews background information on the health and climate effects of particulate matter. In section 4, we describe the CMAQ air quality model, as well as provide an introduction to adjoint models and inverse modeling. Section 5 presents validation results for the adjoint of the aerosol module, as well as the emission sensitivity calculation. $PM_{2.5}$ has been shown to cause various adverse health effects, both short-term and long-term, as well as causing premature mortality. Some studies have suggested that exposure to BC poses a much larger risk to human health than other PM species. We thus consider as an initial application the use of CMAQ adjoint to quantify the impact that emissions in each and every grid cell have on the national health burden attributed to BC exposure (section 6). Lastly, section 7 discusses some conclusions for the current work, as well as provides detail on the future work that will be performed.

3 Background

In this section, we give an overview of particulate matter and its effect on climate and human health. Section 3.1 provides background on size distributions of particulate matter in addition to some of the major sources of these particles. In section 3.2 we present a brief overview of the climate effects (direct, indirect, and semi-direct) of $PM_{2.5}$. Sections 3.3 and 3.4 discuss the short-term and long-term health effects of exposure to $PM_{2.5}$, in addition to discussing the national health burden attributed to exposure to $PM_{2.5}$. Section 3.5 continues the discussion of health effects by discussing the monetary damage values for different $PM_{2.5}$ precursor emissions. In section 3.6, we present information about how emissions are calculated, in addition to some of the uncertainties in the development of emission inventories.

3.1 Particulate Matter

The size distribution of PM is divided into three main modes: coarse, accumulation, and nucleation. The coarse mode consists of particles with an aerodynamic diameter between 2.5 μm and 10 μm ($PM_{2.5-10}$). Particles in the coarse mode are mainly produced by the mechanical break-up of larger particles, have a shorter lifetime in the atmosphere than smaller particles, and usually settle back to the surface due to gravitational forces within minutes to hours. Examples of coarse mode particles are dust, sea salt, plant and insect parts.

The accumulation mode consists of particles with an aerodynamic diameter between 0.1 μm and 2.5 μm ($PM_{0.1-2.5}$). Particles in the accumulation mode are usually coagulated from particles in the nucleation mode. Particles in this mode have the longest lifetime in the atmosphere (days to weeks), and they are hard to remove and do not typically coagulate to the coarse mode.

The nucleation mode consists of particles with an aerodynamic diameter less than 0.1 μm ($PM_{0.1}$). Particles in the nucleation mode are mainly combustion particles that are directly emitted into the atmosphere, or formed from nucleation of vapors during combustion processes. Nucleation mode particles do not settle significantly by gravity. However, particles in this mode are short-lived in the atmosphere and usually coagulate to the accumulation mode. The accumulation mode and nucleation mode are often referred to as fine PM. Ammonium sulfate and ammonium nitrate combine to account for about half of the average mass concentration of fine PM in the U.S., with the rest of the mass concentration coming from carbonaceous aerosols, sodium, chloride, and water (H Seinfeld and N Pandis, 2006).

3.2 Effects of PM on Climate Change

Aerosols have direct, indirect, and semi-direct effects on radiative forcing. Radiative forcing is a perturbation in the radiative energy budget of the Earth caused by an external source (Forster et al., 2007). Aerosols have a direct radiative forcing because they both scatter and absorb solar and infrared radiation in the atmosphere (Boucher et al., 2013). While aerosols in general can cause both a "cooling" and a "warming" effect in the atmosphere, the overall combination of both direct and indirect effects results in the cooling of the atmosphere (Forster et al., 2007).

Indirect Effects Indirect radiative forcing from aerosols is caused by changes in cloud properties. Aerosols alter the efficiency at which liquid water, ice and mixed-phase clouds form and precipitate, which alters the properties of the clouds (Boucher et al., 2013). There is a set amount of water available for clouds. The water can form large droplets within the clouds, which causes precipitation (a major removal mechanism for aerosols). The presence of cloud condensation nuclei in the atmosphere causes the water to condense onto the particles. This results in more, but smaller droplets in the clouds, which increases the cloud albedo (Twomey, 1974). In addition to increasing the albedo, this effect tends to decrease the chance of precipitation. If precipitation is suppressed, this results in excess water remaining in the atmosphere. Atmospheric aerosol particles can also increase the cloud height (Pincus and Baker, 1994).

Semi-Direct Effects While the indirect effects occur when aerosols alter cloud microphysics, absorbing aerosols (AA) near clouds have been thought to cause changes in cloud cover (semi-direct effect) (Hansen et al., 1997). This is caused by the absorbing aerosols within or near clouds increasing the temperature around the clouds, promoting cloud evaporation. A decrease in cloud cover increases the warming impacts of absorbing aerosols, due to the decrease in the amount of solar radiation that is reflected upward by the clouds (cloud albedo effect). Similar studies to Hansen et al. (1997) have shown that this semi-direct effect is enhanced due to a low-cloud feedback loop (Jacobson, 2002) in which the cloud loss increases the capacity for AA absorption.

Arctic Climate Effects In addition to the effects of atmospheric aerosol on radiative forcing, absorbing aerosol that is deposited on snow and ice in the arctic has a substantial effect on climate. The high contrast in albedo between black carbon (BC) and snow or ice on which it has deposited on results in enhanced absorption of sunlight, which heats the Arctic atmosphere and leads to increased melting of snow and ice (Hansen, 2005). The global mean surface temperature warming resulting from the radiative forcing of BC on snow is approximately three times more than an equal forcing of CO_2 (Flanner et al., 2007).

3.3 Health Effects of PM

Exposure to PM in ambient air has been shown to be a cause of various adverse health effects, both short-term and long-term, as well as premature mortality. In 2009 the U.S. EPA released the Integrated Science Assessment for Particulate Matter (PM ISA), which included a literature review of articles that analyzed the health impacts of exposure to PM (EPA, 2009).

Short-Term Exposure In the 2009 PM ISA, articles discussing the effects of short-term exposure to PM were analyzed, and a causal determination was made for various health effects. It was determined that short-term exposure to PM has a causal relationship with cardiovascular effects and mortality, while short-term exposure to PM is likely to have a causal relationship with respiratory effects.

Increases in fine PM and sulfate have been shown to increase mortalities, a majority of which were related to an increase in cardiovascular mortality. The Health Effects Institute

(HEI) performed an extension of a previous American Cancer Society (ACS) study and discovered significant increases in the relative risk of cardiopulmonary and lung cancer deaths, as well as deaths from all causes resulting from exposure to $PM_{2.5}$ (Amann et al., 2006).

Long-Term Exposure Long-term exposure to $PM_{2.5}$ has been shown to have a consistent association with an increased risk of cardiovascular mortality. For example, in a recent extended analysis of the Harvard Six Cities cohort that included an additional 11 years of follow-up and $PM_{2.5}$ data, Lepeule et al. (2012) found that a 10-$\mu g/m^3$ increase in $PM_{2.5}$ resulted in a 14% increased risk of all-cause death (95% CI: 7% to 22%), and a 26% increase in cardiovascular death (95% CI: 14% to 40%). Studies also suggest that long-term exposure to $PM_{2.5}$ is most strongly associated with mortality due to ischemic heart disease, dysrhythmias, heart failure, and cardiac arrest. For these causes of death, an increased $PM_{2.5}$ exposure of 10 $\mu g/m^3$ was associated with an 8-18% increase in death (Pope et al., 2004).

Component-Specific Health Effects Some studies have started focusing on species-specific PM analyses for health impacts. One such study by Bell et al. (2009) analyzed source-specific effects of PM species on both CVD and respiratory diseases. The study found that BC and Vanadium concentration increases resulted in the largest increase in health effect estimates for both CVD and respiratory effects. Bell et al. (2009) showed a 25.8% (95% CI: 4.4 to 47.2) increase in the risk estimate for cardiovascular disease per interquartile range increase in the fraction of BC to $PM_{2.5}$ mass. An increase in interquartile range in the fraction of BC to $PM_{2.5}$ mass was shown to cause a 511% (95% CI: 80.7 to 941) increase in the risk estimate for respiratory disease. Janssen et al. (2011) performed a review of four cohort studies that measured exposure to BC. They calculated a pooled effect relative risk value of 1.007 (95% CI: 1.004 to 1.009) for $PM_{2.5}$, and 1.05 (95% CI: 1.04 1.09) for BC. Such findings suggest that consideration of BC-related health impacts may be of importance.

3.4 Health Burden of Pollutant Exposure

As previously mentioned, exposure to ground-level $PM_{2.5}$ is associated with increased risk of mortality and morbidity. Many studies have estimated the public health burden attributed to exposure to $PM_{2.5}$. Cohen et al. (2005) used economic, meteorologic, and demographic data, as well as available PM measurements in 304 cities, to estimate that 799,000 premature deaths globally were attributed to exposure to urban outdoor air pollution. Anenberg et al. (2010) used simulated global concentrations of $PM_{2.5}$ to estimate the global burden of mortality attributed to exposure to $PM_{2.5}$ from anthropogenic emissions. They estimated that anthropogenic $PM_{2.5}$ was associated with 3,721,000 global premature mortalities annually. Of those premature deaths, 141,000 cardiopulmonary and lung cancer deaths occurred in North America. Fann et al. (2012b) used the CMAQ model in conjunction with observed concentration data to create spatially resolved annual mean $PM_{2.5}$ concentrations over the continental United States. Using this information, as well as the U.S. EPA's BenMAP software, they estimated the total public health burden associated with $PM_{2.5}$ exposure for various risk estimates. They estimated that 130,000 to 320,000 (depending on the risk estimate used) premature mortalities were attributed to $PM_{2.5}$ exposure. They also estimated

an array of morbidity impacts, such as 62,000 hospital admissions related to cardiovascular problems.

A concern with model-based estimates of exposure is model resolution. Punger and West (2013) analyzed the effect of grid resolution on estimates of the burden of fine PM on premature mortality in the USA. They found that coarse grid resolutions (>250km) produce mortality estimates that are 30-40% lower than the estimates at 12-km resolution. They also found that simulations performed at 36-km resolution resulted in mortality burdens 11% higher than at 12-km resolution. While the previous studies have shown that exposure to $PM_{2.5}$ results in a large number of premature mortalities, it is important to determine which emissions (location and sector) have the largest effect on human health.

3.5 Damages of Pollutant Exposure

When calculating damages associated with pollutant exposure, a value of a statistical life (VSL) is used to convert from mortalities to a monetary value. Muller and Mendelsohn (2007) used an integrated assessment model to estimate the marginal damages associated with emitting an additional ton of pollution from approximately 10,000 sources in the U.S.. They estimated that $PM_{2.5}$ emissions account for $17.4 billion of gross annual damages (GAD) per year. Muller et al. (2011) again used an integrated assessment model to estimate the gross damages for each industry in the U.S. They estimated that a total of $184 billion of gross external damages (GED). For both of these studies a fixed damage value was used throughout the domain.

Fann et al. (2009) examined how the location and source of an emission reduction influence the magnitude of the benefit per ton ($/ton) estimate for $PM_{2.5}$ reductions. Using a reduced-form air quality model, they modeled emission control strategies for each of nine urban areas. They showed that the $/ton for some pollutants are much higher than others. They also showed a large variability in $/ton estimates for the same pollutant across various sources and locations. Fann et al. (2012a) used the CAMx source apportionment photochemical model to estimate $PM_{2.5}$ benefit per ton estimates for seventeen sectors across the continental U.S. They estimated that the benefit per ton of reducing directly emitted $PM_{2.5}$ is an order of magnitude larger than reducing precursor emissions.

Additionally, in 2011 the U.S. EPA released a report analyzing the benefits and costs of the Clean Air Act from 1990 to 2020 (EPA, 2011). They estimated that the costs of efforts to meet the 1990 Clean Air Act Amendment are projected to cost about $65 billion annually. However, the value of the improvements resulting from these effort are estimated to reach approximately $2 trillion, with a majority of the benefits coming from mortality reduction (approximately $1.8 trillion of the $2 trillion total benefits). To achieve the highest benefit to cost ratio, it is necessary to determine the emissions to which stricter control strategies would yield the largest reduction in premature mortalities associated with pollutant exposure.

3.6 Emissions and Uncertainty

When using atmospheric chemical transport models to evaluate air quality and climate issues, a vast array of input information is required, including emission profiles. However, emission inventories are subject to substantial levels of uncertainty, which limits the confidence that

can be placed in results that are based on them. In the US, the National Emission Inventory (NEI) is a compilation of emission profiles from state, local, and tribal air agencies, as well as the emission information from EPA emission programs. NEI emission inventories include criteria air pollutants (CAPs), pollutants related to the implementation of NAAQS, as well as hazardous air pollutants (HAPs) that are associated with EPA's Air Toxics Program. CAPs include lead, carbon monoxide, nitrogen oxides, volatile organic compounds, sulfur dioxide, ammonia, and particulate matter. HAPs include 187 other pollutants, such as mercury, hydrochloric acid, and heavy metals. The emission sources are divided into categories: stationary sources are "point" or "nonpoint", mobile sources are either onroad (cars and trucks driven on roads) or non-road (locomotives, aircraft, marine, etc.).

Emissions for various sectors at various locations are calculated based on emission factors. An emission factor is a value that attempts to relate the quantity of a pollutant released to the activity that releases the pollutant. Emission factors are generally expressed as a weight of pollutant divided by a unit weight, volume, distance, or duration of the activity that is emitting the pollutant. In most cases, the emission factors are simply an average of all available emission profile data. Emissions are then calculated by

$$E = A * EF * (1 - \frac{ER}{100}) \tag{1}$$

where E is the calculated emissions, A is the activity rate, EF is the emission factor, and ER is the overall emission reduction efficiency.

Power plant emission profiles tend to have very low uncertainty. This is a result of the availability of a large number of detailed, hourly emission data that are a product of the continuous emissions monitoring system (CEMS). Mobile source inventories contain significant uncertainties with regard to the magnitude of CO and NO_x emissions (Fujita et al., 2012). Much of the mobile-source tailpipe emissions data are typically estimated based on procedures that are of a limited duration. The short-term tests may not accurately represent the emissions over longer time periods. Also, the effects of emission spikes that result from variability in engine loads are not accurately represented (Hallmark et al., 2002).

Emissions from nonpoint stationary sources (fugitive emissions, open biomass burning, etc.) have a high level of uncertainty. There are many causes for the high level of uncertainty in nonpoint stationary sources. The individual sources may be small and widely dispersed (Hanna and Wilkinson, 2004), or in the case of fugitive emissions, they may result from unknown sources. The uncertainty for the isoprene emission factor is reported as $\pm 50\%$ (Hanna et al., 2002). Also, in cases such as agricultural-related ammonia, biomass burning, and biogenic emissions, emissions may be from processes that contain inherent variability. For example, considerable uncertainties remain in determining the burned area for biomass burning. Also, many fires cannot be observed during the flaming stage due to obstruction in the satellite view (such as from cloud coverage) (Bond et al., 2013). The use of observations to constrain emissions is thus an important, developing topic for aerosol modeling.

4 Methods

In air quality studies, we are concerned with a wide variety of topics such as determining the sources that have the largest contributions to pollutants in an area, determining the most cost-effective way to reduce pollutant concentrations, and determining where to place a future source in order to minimize its environmental impacts. Air quality models that involve descriptions of emission patterns, meteorology, chemical transformations, and removal processes are essential for answering these questions. Here we describe the CMAQ model and its adjoint.

4.1 CMAQ Model

The air quality model currently used by the EPA is the CMAQ modeling system (Appel et al., 2007). It is designed to approach air quality as a whole by modeling multiple air quality issues. CMAQ is a three-dimensional Eulerian chemical transport model of gaseous and aerosol air pollution. CMAQ is developed to have multi-scale capabilities so that separate models are not required for urban scale and regional scale air quality modeling.

The CMAQ model consists of horizontal advection and diffusion, vertical advection and diffusion, gas-phase chemistry, aerosol microphysics, and cloud processes (including wet deposition and aqueous chemistry). In version 4.7.1 of the CMAQ model (the version that the adjoint is developed from), both the piecewise parabolic pethod (ppm) and global mass-conserving (yamo) advection schemes are supported. The yamo method uses the ppm scheme for horizontal advection, and derives a vertical velocity component at each grid cell that satisfies the continuity equation using the driving meteorology model's density. This version of the model uses the ACM2 PBL model (Pleim, 2007). The ACM2 model is able to represent both the supergrid and subgrid-scale components of turbulent transport in the convective boundary layer.

CMAQ v4.7.1 allows the user to choose either the CB05 chemical mechanism or the SAPRC99 chemical mechanism. Some of the differences between the CB05 and SAPRC99 mechanisms are that they use a different scheme for condensing the organic chemistry, and the SAPRC99 mechanism has more detailed organic chemistry than CB05. The cloud processes model includes aqueous chemistry and wet deposition. Wet deposition is calculated for both subgrid-scale convective clouds, as well as resolved clouds. The CMAQ aerosol module is detailed in the next section.

4.2 CMAQ Aerosol Module

CMAQ version 4.7.1 utilizes a new aerosol module called AERO5. The AERO5 module employs a modal approach to represent the size distribution of particulate matter (Binkowski and Roselle, 2003; Mebust et al., 2003). The particle size distribution is represented as a superposition of three lognormal sub-distributions, called modes: Aitken mode, accumulation mode, and coarse mode. In the default configuration, CMAQ estimates concentrations of aerosols in each of the three modes (e.g., ASO4I, ASO4J, ASO4K correspond to sulfate aerosol in the Aitken mode, accumulation mode, and coarse mode, respectively). All three modes are subject to wet and dry deposition, in addition to condensation.

The AERO5 modules solves the general dynamic equation for aerosols:

$$\begin{aligned}\frac{\partial}{\partial t}n(v,t) = &\frac{1}{2}\int_0^v K(v-q,q)n(v-q,t)n(q,t)dq \\ &- n(v,t)\int_0^\infty K(q,v)n(q,t)dq \\ &- \frac{\partial}{\partial v}(I(v)n(v,t) + J_0(v)\delta(v-vo) + S(v) + R(v)\end{aligned} \tag{2}$$

where the first term on the right hand side corresponds to the formation of particles of volume v from coagulation, the second term corresponds to the loss of particles of volume v, the third term corresponds to condensation and evaporation, the fourth term corresponds to the formation of particles of volume v by nucleation, $S(v)$ are sources, and $R(v)$ are removals (deposition). $n(v,t)$ is the particle number distribution, K is the coagulation coefficient, $I(v)$ is the condensation growth rate, and $J_0(v)$ is the nucleation rate. Equilibrium concentrations of inorganic aerosols are solved using ISORROPIA II (Fountoukis and Nenes, 2007).

While previous versions treated all secondary organic aerosol (SOA) as semi-volatile, the AERO5 module has the following four types of non-volatile SOA:

1. SOA formed by in-cloud oxidation from glyoxal and methyglyoxal.
2. Enhancement of isoprene-derived SOA under acidic conditions.
3. SOA originating from aromatic oxidation under low-NO_x conditions.
4. Oligomerization of particle-phase semi-volatile organic material.

Previous versions of CMAQ considered coarse-mode particles to be dry and inert. Additionally, components in the coarse mode could not evaporate or condense. CMAQ version 4.7, however, allows semi-volatile aerosol components to condense and evaporate from the coarse mode and non-volatile sulfate to condense on the coarse mode. CMAQ version 4.7 also uses dynamic mass transfer to simulate the coarse mode. This is because particles in the coarse mode are often not in equilibrium with the gas-phase.

4.3 CMAQ $PM_{2.5}$ Evaluation

With the release of each new version of the CMAQ model, the U.S. EPA also releases documentation evaluating the performance of the model. The evaluation typically involves the comparison of modeled concentrations of $PM_{2.5}$ (speciated, or as a whole) and select gaseous species to observations from the IMPROVE, CASTNet, STN, and SEARCH monitoring networks.

Appel et al. (2008) analyzed the model performance of CMAQv4.5 for various PM species. Comparing modeled concentrations for 2001 to CASTNet, STN, and IMPROVE observations showed a good performance for SO_4^{2-}, with normalized mean bias ranging from 0.2% (CASTNet) to 10.1% (STN) for 12-km domains. Model performance for NH_4^+ is also good for all seasons except for the fall. For much of the year, comparing model performance of

ammonium to observations yielded normalized mean bias around -10% for CASTNet, and about 20% for STN. However, in the fall, ammonium concentrations are over predicted, with a normalized mean bias of up to 170%. Particulate NO_3^- is consistently over predicted in the winter and spring, and under predicted in the summer, with a normalized mean bias of about -50% for the summer months. Overall model performance of elemental carbon is reasonably well, although the biases are small due to small observed concentrations of BC. There is, however, a small under prediction of BC in the summer months.

Appel et al. (2012) again analyzed the model performance of CMAQ, but this time looked at $PM_{2.5}$ as a whole for CMAQv4.7.1 over North America. It was shown that CMAQ does a good job of estimating $PM_{2.5}$ in the summer in the U.S. (normalized mean bias of -4.6%), but the model overestimates concentrations in the rest of the year, with a normalized mean bias ranging from 18.9% (Spring) to 36.3% (Fall). PM_{10} is consistently underestimated for all seasons, with normalized mean bias ranging from -46.5% to -64.8%.

4.4 Adjoints and Inverse Modeling

Inverse modeling is a means by which one can constrain model parameters (in this case, aerosol precursor emissions) through the use of observational data. 4-D variational data assimilation provides a framework for combining observations and models to make an estimate of a system (in this case, the chemical makeup of the atmosphere). In order to quantify the misfit between the model prediction and the observed data, a cost function is introduced

$$J(\boldsymbol{\sigma}) = \frac{1}{2}\sum_{c\in\Omega}(H\mathbf{c} - \mathbf{c}_{obs})^T\mathbf{S}_{obs}^{-1}(H\mathbf{c} - \mathbf{c}_{obs}) + \frac{1}{2}\gamma(\boldsymbol{\sigma} - \boldsymbol{\sigma}_a)^T\mathbf{S}_a^{-1}(\boldsymbol{\sigma} - \boldsymbol{\sigma}_a). \tag{3}$$

The parameter H is the observation operator, $\mathbf{c}_{obs}$ is the vector of species observations, $\mathbf{S}_{obs}$ is the error covariance matrix of the observations, γ is a regularization parameter, $\boldsymbol{\sigma}_a$ is the a priori estimate of the control variables, $\mathbf{S}_a$ is the error covariance estimate of the control variables, Ω is the domain over which observations and model predictions are available, and $\boldsymbol{\sigma}$ is the solution that minimizes the cost function. An adjoint model is a means of calculating the sensitivity of the cost function with respect to all model parameters simultaneously. This approach to inverse modeling is appealing because it allows for both the overall magnitude and spatial distribution of emission to be refined (Henze et al., 2009).

Following the derivation by Giering and Kaminski (1998), the derivative of the cost function with respect to the vector of initial conditions is

$$\nabla_{c^0} J(\boldsymbol{\sigma}) = A^*(\boldsymbol{\sigma})(F(\boldsymbol{\sigma}) - D), \tag{4}$$

where $A^*(\boldsymbol{\sigma})$ represents the adjoint model, $F(\boldsymbol{\sigma})$ is the model output, D is a set of observations, and the difference $(F(\boldsymbol{\sigma}) - D)$ is often referred to as the adjoint forcing. This can be extended to calculate the derivative of the cost function with respect to the control variables by

$$\nabla_{\boldsymbol{\sigma}} J = \left(\frac{\partial \underset{\sim}{c}}{\partial \boldsymbol{\sigma}}\right)^T \frac{\partial J}{\partial \underset{\sim}{c}} \tag{5}$$

It has been shown that the computation of the cost function and its gradient, in general, takes only two to five times the computation of the cost function (Baur and Strassen, 1983; Griewank, 1992). The gradient vector $\nabla_{\boldsymbol{\sigma}} J(\boldsymbol{\sigma})$ could also be calculated using the finite difference method. However, the adjoint method has two main advantages over the finite difference method:

1. Especially for a large number of parameters, n, the adjoint model saves run time. The adjoint model takes approximately $\frac{5}{2n}$ the run time of the finite difference method.
2. The computed gradient is exact when using the adjoint model.

Adjoints of Eulerian chemical transport models have been developed and used for inverse modeling of emissions (e.g., Elbern et al. 2000; Hakami et al. 2005; Henze et al. 2007; Martien and Harley 2006). Most emphasis to date in chemical data assimilation studies has been on gas-phase species. An adjoint of a fixed size aerosol model has been developed for a global coupled chemistry-aerosol model (Henze et al., 2007) and box model adjoint of aerosol dynamics have been studied (Henze et al., 2004; Sandu et al., 2005). Dubovik et al. (2008) developed the adjoint of the GOCART aerosol transport model to retrieve global aerosol source emissions from satellite observations. Huneeus et al. (2009) developed a simplified aerosol model, and its adjoint in order to optimize global aerosol and aerosol precursor emissions using variational data assimilation. Inclusion of aerosol-phase chemistry in the existing CMAQ-ADJ will result in the first coupled gas-aerosol, regional scale adjoint model to explicitly describe aerosol mass composition and size distribution.

For this project, we have developed the adjoint of a majority of the aerosol microphysics code, in addition to implementing the calculation of emission sensitivities. The adjoint of the secondary organic aerosol module within the aerosol code, in addition to the adjoint of the aerosol module driver and nucleation processes were developed by ShunLiu Zhao at Carleton University. The adjoint of all transport routines were updated from a previous version of the gas-phase adjoint model (Hakami et al., 2007) by Peter Percell at the University of Houston. As of writing this, the adjoint of gas-phase chemistry and aqueous chemistry are being developed by Amir Hakami's group at Carleton University.

5 CMAQ Adjoint Validation

An adjoint of the entire AERO5 module in CMAQ has been developed. In order to verify that the adjoint has been correctly derived, one needs to compare the calculated adjoint sensitivities to another form of sensitivity calculation. The validation performed for this project compares adjoint sensitivities to first-order finite difference sensitivities, with varying percentage perturbations. First-order finite difference (FD) sensitivities are calculated by

$$\frac{\partial f}{\partial x} = \frac{f(x+h) - f(x)}{h} \tag{6}$$

where $f(x)$ is the concentration output from the default inputs, h is the perturbation, and $f(x+h)$ is the concentration output from the perturbed inputs. One problem with the

finite difference approximation is the dependence on the perturbation size. Choosing a perturbation that is too small can result in errors due to subtractive cancellation. However, perturbation sizes too large can result in truncation error.

For certain cases where finite difference calculations do not provide correct sensitivities, complex variable sensitivities were used in order to confirm that the adjoint is providing correct results. Complex variable sensitivities are calculated by

$$\frac{\partial f}{\partial x} \approx \frac{Im[f(x+ih)]}{h} \tag{7}$$

The complex variable estimate is not subject to subtractive cancellation, since it does not involve a difference operation. In order to compute complex variable sensitivities for the CMAQ model, the entire model (or part of the model that is being validated) must be modified to perform all calculations with complex numbers, as opposed to real numbers. Simulations performed with complex arithmetic not only have longer runtimes, but also use approximately double the memory requirements.

When performing the adjoint validation simulations, gradient data was generated for the entire U.S. domain at a 36-km resolution. Simulations were run for varying durations (ranging from 1 timestep simulations to 1-day simulations) using inputs for April 03, 2008. In an effort provide a more physically-relevant initial condition profile, a spin-up simulation was performed, running from April 01, 2008 through April 02, 2008. However, for certain cases it was necessary to replace initial concentrations for some species with larger values. For example, after the two day spin-up simulation certain species still had concentrations of 1.0E-30 $\mu g/\mathrm{m}^3$. Applying any percentage perturbation smaller than 100% to a value this small results in an incorrect sensitivity value of 0, due to the fact that the perturbation is outside the numerical precision of the computer.

5.1 Aerosol Module Validation

For Figures 1 and 2, sensitivities are calculated for the list of species given in Table 1.

When performing finite difference sensitivity calculations, we found it best to not include aerosol thermodynamics (ISORROPIA) in the aerosol module. ISORROPIA is a highly nonlinear, discontinuous aerosol thermodynamics model, which is subject to substantial cancellation errors when sensitivities are calculated with the finite difference method. ANISORROPIA (the adjoint of ISORROPIA), however, has been validated by comparing adjoint sensitivities to complex variable sensitivities (Capps et al., 2011). Therefore, we can generate finite difference sensitivities of the aerosol adjoint without ISORROPIA and still be confident in the accuracy of the full aerosol adjoint.

Series of simulations were run with different forcings (adjoint) and perturbations (finite difference) in order to generate partial Jacobian data for aerosol-only simulations without ISORROPIA. When comparing the adjoint Jacobian (Figure 1(a)) to the FD Jacobian (Figure 1(b)) for two timesteps, it is evident that while the sensitivities are comparable for many relationships, there are some relationships for which the adjoint and FD do not match. Specifically, instances with accumulation mode sodium (ANAJ) in the denominator show sensitivities of zero for FD, while the adjoint provides non-zero values. Additionally, the

NO2	Nitrogen Dioxide
N2O5	Dinitrogen Pentoxide
HNO3	Nitric Acid
HCL	Hydrochloric acid
ASO4J	Accumulation mode sulfate aerosol
ASO4I	Aitken mode sulfate aerosol
ANH4J	Accumulation mode ammonium aerosol
ANH4I	Aitken mode ammonium aerosol
ANO3J	Accumulation mode nitrate aerosol
ANO3I	Aitken mode nitrate aerosol
AECJ	Accumulation mode elemental carbon
AECI	Aitken mode elemental carbon
AH2OJ	Accumulation mode water aerosol
AH2OI	Aitken mode water aerosol
ANAJ	Accumulation mode sodium aerosol
ACLJ	Accuulation mode chlorine aerosol
ACLI	Aitken mode chlorine aerosol
NH3	Ammonia

Table 1: List of species used in Jacobian sensitivity calculations

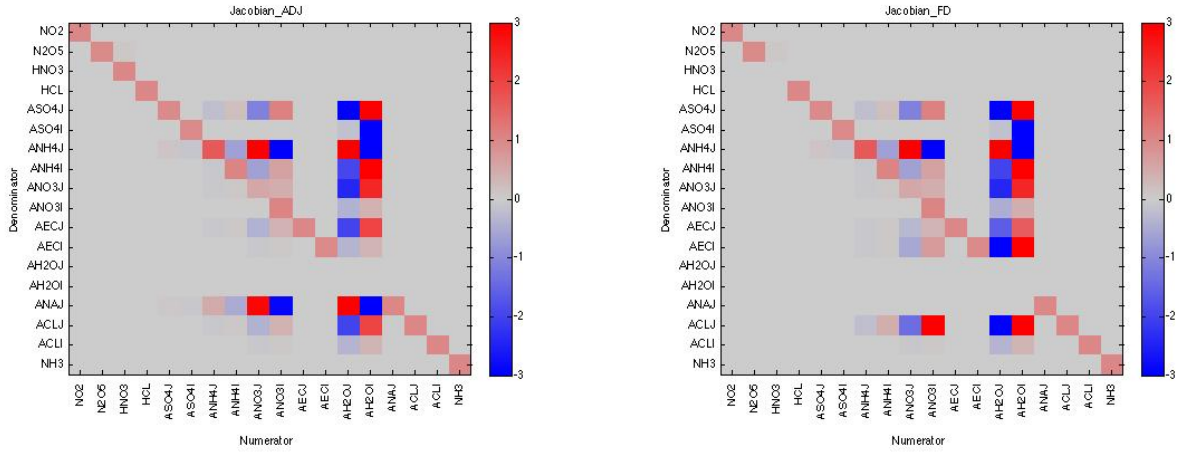

(a) (b)

Figure 1: Partial Jacobian plots of (a) adjoint sensitivities and (b) FD sensitivities for aerosol-only simulations without aerosol thermodynamics. Simulations were run for two timesteps.

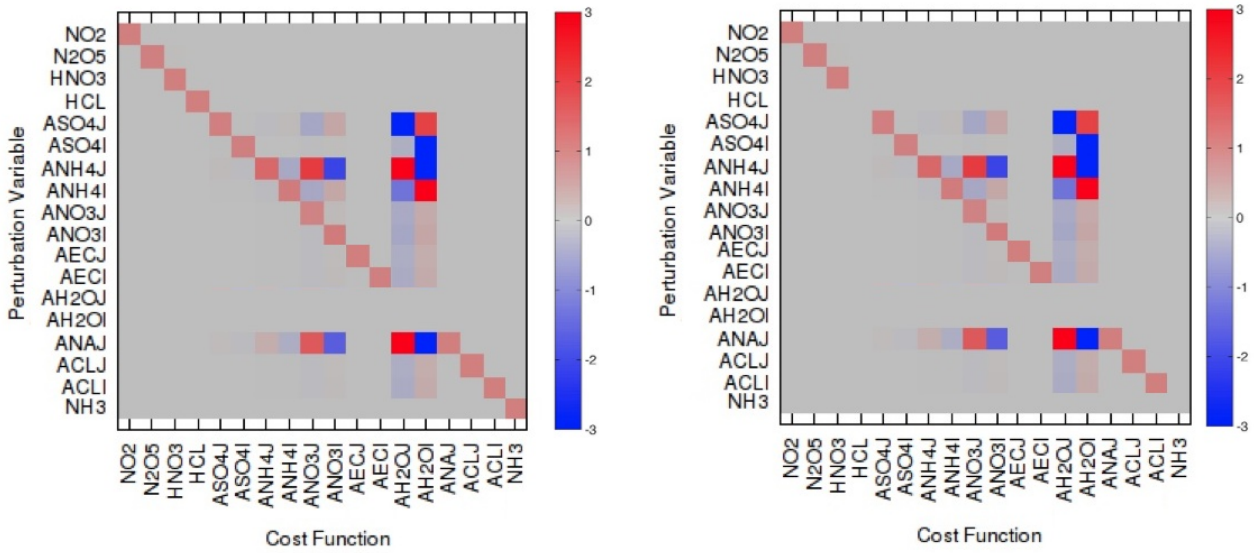

(a) (b)

Figure 2: Partial Jacobian plots of (a) adjoint sensitivities and (b) CVM sensitivities for aerosol-only simulations that exclude aerosol thermodynamics. Simulation was run for one timestep.

sensitivity of nitric acid (HNO_3) with respect to nitric acid shows a sensitivity of zero in the FD test, yet shows a value of approximately one in the adjoint.

The differences between adjoint and finite-difference sensitivities are most likely attributable to failure of the finite-difference simulations to accurately calculate the sensitivities. In order to confirm this, similar tests were performed comparing adjoint sensitivities (Figure 2(a)) to complex variable method (CVM) sensitivities (Figure 2(b)), however for a single timestep. Simulations to generate the CVM partial Jacobian were performed by Shunliu Zhao at Carleton University.

From Figure 2 it is apparent that the zero sensitivity values with ANAJ in the denominator in the previous figure (Figure 1) are attributed to a failure in the FD calculations. Additionally, for this specific configuration of the aerosol module, it can be determined that the aerosol module is behaving properly. However, there are still a few instances where the adjoint and CVM sensitivities do not match; specifically, sensitivities of NH_3 with respect to NH_3, and sensitivities of HCL with respect to HCL, where the adjoint provides sensitivities of one, and the CVM provides sensitivities of zero. However, the finite difference calculations provide values of one for these relationships. One would expect the sensitivity of a species to itself to be one for a single timestep, hence the disagreement between adjoint and CVM sensitivities for these cases is likely owing to an error in the CVM calculation.

5.2 Emission Sensitivity Validation

By default, the CMAQ adjoint calculates the sensitivity of a given cost function with respect to concentrations. While sensitivities with respect to concentrations provide vital information for many studies, there are a large number of applications that require sensitivities with respect to emissions. As with the development of the aerosol adjoint, the inclusion of emission sensitivity calculation requires its own validation tests.

As opposed to the validation of the aerosol module, the validation of the emission sensitivity calculation cannot simply treat the domain as an array of box models. Within the CMAQ model, the injection of emissions into the model occurs in the vertical diffusion (VDIFF) module. The VDIFF module transports concentrations vertically between layers. Because of the transport between layers, validation of the vertical diffusion (VDIFF) and vertical advection (ZADV) was performed for simulations where the domain was treated as an array of column models.

For the first-order finite difference sensitivity calculations of BC with respect to BC emissions, a 0.01% perturbation was applied to concentrations in entire columns. After allowing the simulations to run for four hours, scaled sensitivity values were calculated by dividing the change in output concentrations in a single layer by the emissions scaling factor, or perturbation ($\frac{\Delta Conc}{SF_{emis}}$). On the other hand, semi-normalized adjoint sensitivities were calculated by applying a forcing in a single layer (the same layer for which concentrations were analyzed in the finite difference calculations) at the end of the four hour simulation and then looking at output sensitivity values summed over the entire column, scaled by the emissions ($\frac{\delta J_{layer}}{\delta emis} * emis$). Since every layer between layer two and TOA are handled the same within the vertical transport code, it is only necessary to validate one of these layers in order to confirm the accuracy of the adjoint code.

Initial emission sensitivity validation was performed for a configuration that included only vertical diffusion (VDIFF) and vertical advection (ZADV). Since the vertical layer closest to the surface (layer one) is handled separately from the rest of the vertical layers, validation tests were performed for two different layers, layer one (Figure 3(a)) and layer twelve (Figure 3(b)).

One can see from Figure 3 that the adjoint gradients match the finite difference gradients for both layer one and layer twelve nearly perfectly. For the validation of both layers, we have an R^2 value that is nearly one. Additionally, the scatter plots show that all points lie essentially on the one-to-one line. Because of this, we can conclude that the calculation of sensitivities with respect to emissions has been properly implemented.

In addition to the above validation tests that were performed with a model configuration that included only VDIFF and ZADV, validation of sensitivity with respect to emissions were also performed for a configuration that included the aerosol module (AERO5, VDIFF, ZADV). As in the validation above, validation tests for this configuration were performed for both layer one (Figure 4(a)) and layer twelve (Figure 4(b)).

Again, it can be seen from Figure 4 that the adjoint gradients match the finite difference gradients nearly perfectly for both layers. For the configuration that includes the AERO5 module the agreement between adjoint and FD sensitivities for layer one is slightly worse,

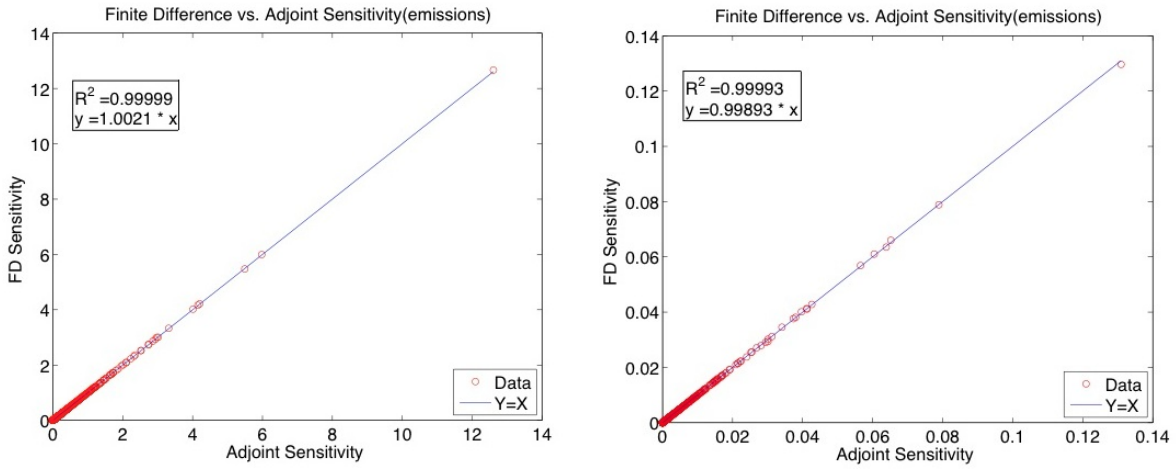

(a) (b)

Figure 3: Finite Difference $\frac{\Delta Conc}{SF_{emis}}$ vs. Adjoint emission sensitivity ($\frac{\delta AECJ}{\delta AECJ} * emis$) for (a) layer 1, and (b) layer 12. Model configuration included only VDIFF and ZADV.

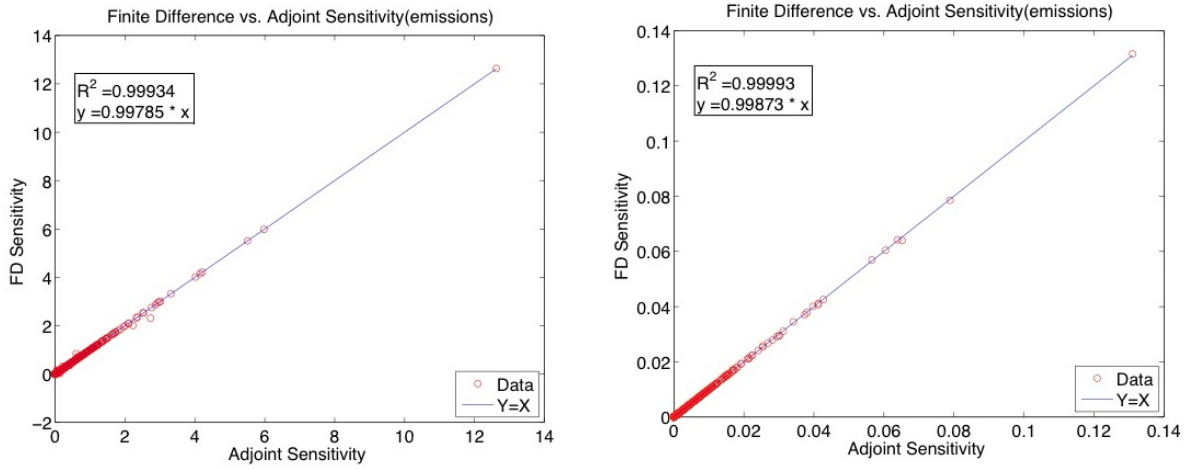

(a) (b)

Figure 4: Finite Difference $\frac{\Delta Conc}{SF_{emis}}$ vs. Adjoint emission sensitivity ($\frac{\delta AECJ}{\delta AECJ} * emis$) for (a) layer 1, and (b) layer 12. Model configuration included VDIFF, ZADV, and AERO5.

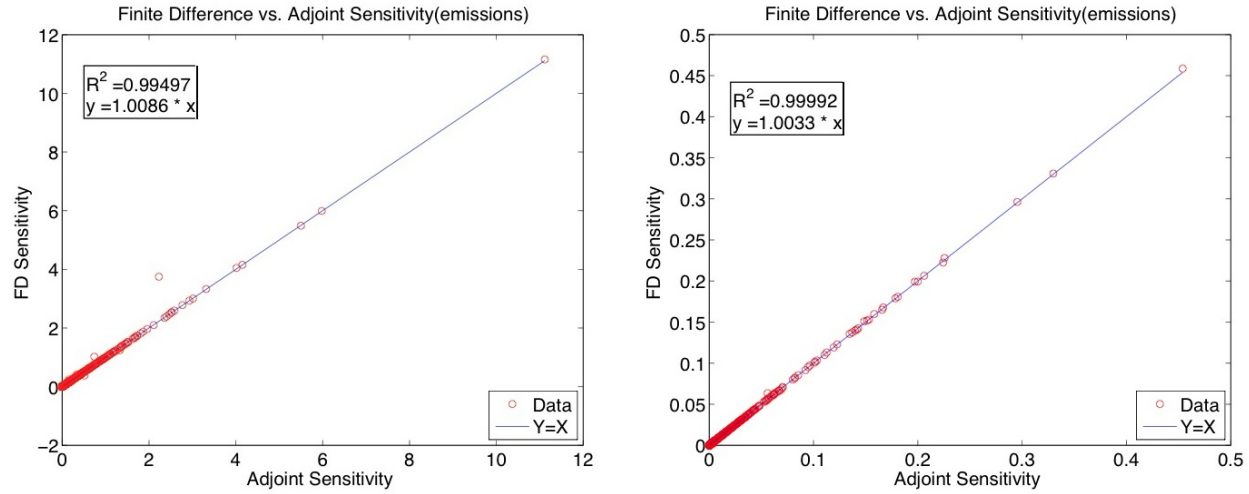

(a) (b)

Figure 5: Finite Difference $\frac{\Delta Conc}{SF_{emis}}$ vs. Adjoint emission sensitivity ($\frac{\delta AECJ}{\delta AECJ} * emis$) for (a) layer 1, and (b) layer 8. Model configuration included VDIFF, ZADV, AERO, and CLOUDS.

with a few points falling off of the one-to-one line. However, the R^2 value is still nearly one and the points not on the one-to-one line are very close to lying on the line. Based on these emission sensitivity comparisons with the inclusion of the AERO5 module, it can be determined that the emissions sensitivity calculation has been implemented correctly. It can also be determined that the aerosol module is correctly coded for sensitivities of BC with respect to BC.

Working towards a full model validation, another validation test was performed for a model configuration that included CLOUDS into the previous configuration. For this configuration validation was again performed for two separate layers. However, validation tests were performed for layer one (Figure 5(a)) and layer eight (Figure 5(b)), as opposed to layer twelve.

It can be determined from Figure 5 that, in addition to emissions sensitivity calculations being properly implemented, the cloud adjoint module is also correctly written for BC processes. The adjoint and finite difference sensitivities again match nearly perfectly for both layers, however the first layer scatterplot now contains a few points that are off the one-to-one line, one of which has a FD sensitivity value that is approximately 165% that of the adjoint sensitivity (FD $\approx$ 3.8, ADJ $\approx$ 2.3). This is most likely caused by nonlinearities in the model causing the finite difference calculation to result in an incorrect sensitivity value.

6 Health Impacts of BC Emissions

In this section we use adjoint sensitivities to attribute national mortality from exposure of BC to BC emissions. When running an adjoint simulation, we first need to define the cost function and adjoint forcing equations (Section 6.1). We then provide information about the

inputs used in the forward and adjoint simulations (Section 6.2), the model configuration (Section 6.3), and forward simulation results (Section 6.4). The resulting sensitivities from the adjoint simulations are then analyzed in multiple fashions: sensitivities to anthropogenic emissions (Section 6.5.1), and sensitivities to anthropogenic emissions on a per state basis (Section 6.5.2).

6.1 Cost Function for National Mortalities

It was determined from the tests in section 5.2 that the adjoint model is sufficiently validated to allow for application of the tool to focus on simulations specific to BC. In this section we define the cost function (J) to be the following health impact function:

$$J = \sum_{i=1}^{N} Mort_i * (1 - \exp^{-\beta * Conc_i}) \tag{8}$$

where *Mort* is the gridded annual mortalities in the U.S., t is the number of model time steps in a year, *Conc* is the gridded annual average BC concentration, i is the grid cell index, N is the total number of grid cells for which the cost function is to be calculated, and β is the concentration response factor. For this study we used a concentration response factor of 0.005827, which was calculated from the relative risk value presented by Krewski et al. (2009).

The adjoint forcing (Equation 9), which is what drives the adjoint model, was then calculated by taking the derivative of the cost function with respect to concentration,

$$\frac{\partial J}{\partial Conc} = \frac{Mort}{t} * \beta * \exp^{-\beta * Conc}. \tag{9}$$

Mortality rates were obtained from BenMAP simulations that used mortality data from 2004-2006 from the Centers for Disease Control and National Center for Health Statistics (Abt, 2013. Bethesda, MD.).

6.2 CMAQ Meteorology and Emissions

Meteorological inputs for the continental U.S. were obtained from version 3.1 of the Weather Forcasting Model (WRF). This provides hourly-varying horizontal wind components, temperature, moisture, vertical diffusion rates, and rainfall rates for each grid cell in the CMAQ model domain. The boundary conditions and initial condition profiles were obtained by running GEOS-Chem version 8.02.03 with a grid resolution of 2.0°x 2.5°and 47 vertical layers (GEOS-Chem simulations were performed by Harvard University). The boundary condition profiles were calculated at three-hour intervals.

The emission inputs used version 2 of the 2008 National Emission Inventory (2008 NEI) as a starting point. The 2008 NEI includes five data categories: non point sources, point sources, nonroad mobile sources, onroad mobile sources, and fires. The 2007 emissions also included biogenic emissions (obtained from the BEIS3.14 model), emissions from Canada's 2006 inventory and Mexico's Phase III 2008 inventory. Wildfire emissions were calculated using the SMARTFIRE2 system. The SMARTFIRE2 system categorizes all fires as either

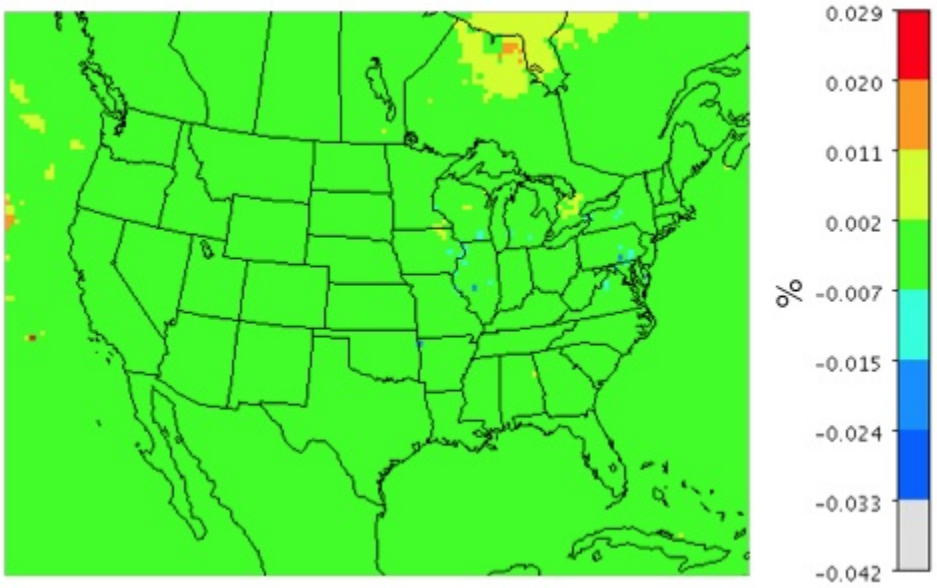

Figure 6: Percent difference in mean BC average surface concentrations for simulations with and without gas-phase chemistry for a 2-day simulation duration.

prescribed or wildfire burning, and includes improved emission factor estimates for prescribed burning.

6.3 Model Setup

Forward model simulations were run from December 21, 2006 to December 31, 2007 to generate gridded average concentrations for the year to be used in the health impact function (Equation 8). Adjoint simulations were run for 12 1-week periods, from the 1st to the 7th of each month. The modeling domain covers the continental United States, northern Mexico, and southern Canada. The horizontal domain is a 12km resolution domain consisting of 396 $\times$ 246 grid cells. The vertical domain consists of 24 terrain-following layers in sigma-pressure coordinates.

We performed simulations for CMAQ model configurations that did not include gas-phase chemistry, as the adjoint of the gas-phase chemistry module has yet to be fully validated. However, in order to conclude that the results from this study are stable without gas-phase chemistry, it was necessary to analyze the effect that the inclusion of the gas-phase chemistry module has on simulated BC concentrations. Simulations were run for a two-day time period for two configurations: one with gas-phase chemistry, and one without gas-phase chemistry. The simulated hourly concentrations of BC were averaged over the two-day simulation period, and the percentage difference was plotted for the entire CMAQ model domain. From Figure 6, it is apparent that the gas-phase chemistry module has a negligible effect on simulated BC concentrations. This makes sense, since BC is inert.

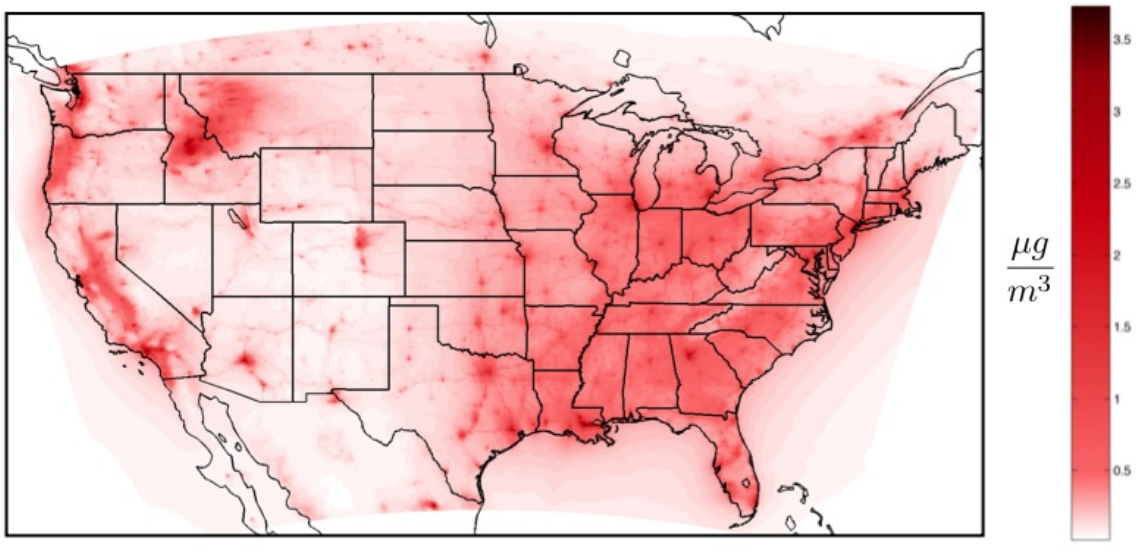

Figure 7: Gridded annual average BC concentrations.

6.4 Forward Model Simulations

As mentioned in Section 6.3, forward model simulations were performed for 2007 in order to generate yearly average concentrations (Figure 7). The annual average BC data was then used in the health impact function (Equation 8) in order to calculate the mortalities attributed to exposure to BC for 2007.

Figure 8 shows the gridded mortalities calculated using the yearly average BC concentration. The figure shows, as one might expect for short-lived species, that a majority of mortalities attributed to exposure to BC occur around major cities. From the cost function (Equation 8), we estimate approximately 12,583 national mortalities attributed to exposure to BC for 2007. This is consistent with previous studies (see section 3.4), taking into account that about 5-10% of $PM_{2.5}$ mass is BC (Sasser et al., 2011).

6.5 Results

Semi-normalized sensitivities ($\frac{\partial J}{\partial Emis} * Emis$, Figure 9) with respect to emissions scaling factors (referred to as *contributions*) were accumulated throughout the entire week of the adjoint run, and the resulting sensitivities were averaged over the 12 individual simulations. The average sensitivity was then appropriately scaled based on the assumption that the 12 individual weeks combine to accurately represent the year as a whole.

For the results presented in this section, contribution percentage is defined as the fraction of contribution from anthropogenic (Section 6.5.1) or biomass burning (Section 6.5.3) emissions in a single grid cell over the sum of contribution from all emissions, converted to percentage. Mortality percentage is the mortality in a single grid cell divided by the total number of mortalities in the U.S., converted to percentage.

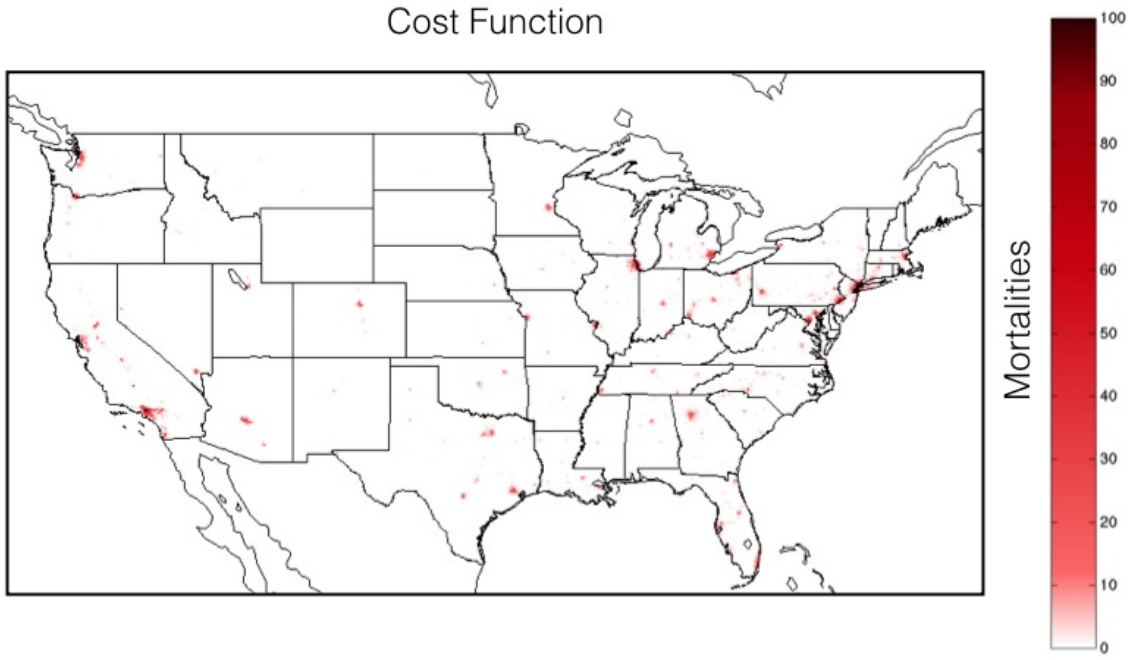

Figure 8: Gridded annual premature mortalities associated with exposure to BC concentrations.

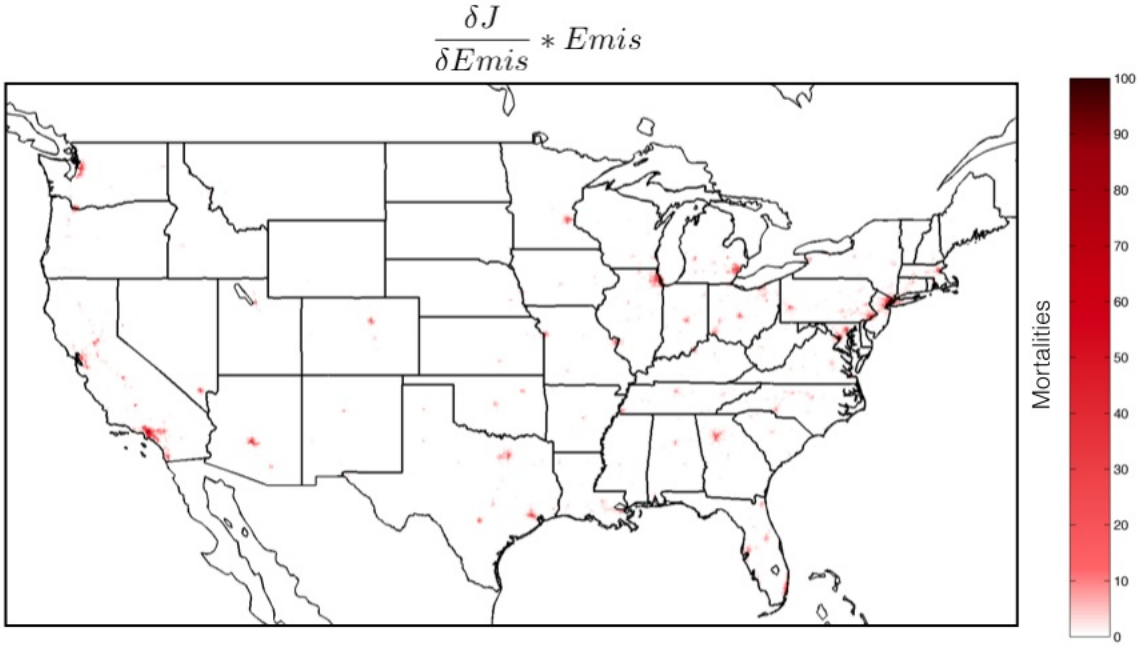

Figure 9: Semi-normalized sensitivities ($\frac{\partial J}{\partial Emis} * Emis$) showing the sensitivity of national mortality to emissions in each grid cell. A maximum of 174.2 mortalities are attributed to BC emitted from New York, NY.

6.5.1 Sensitivity of BC Health Effects to Anthropogenic Emissions

We have generated figures for various ratios (contribution percentage over emission percentage, etc.) on a log scale. When generating these ratio plots, not all information was included. Of the 97,000+ grid cells in the domain, data from only approximately 10,000 grid cells were used. For each ratio plot, the largest 5,000 values for the numerator and denominator are displayed in the plot. For example, if plotting the ratio of contribution percentage over mortality percentage, the 5,000 grid cells with the largest contribution percentage as well as the 5,000 grid cells with the largest mortality percentage are plotted.

We chose to only plot a subset of the grid cells in order to emphasize the cells with larger values, while also omitting cells that might have large ratios but small overall impacts. For comparison, Figure 10 shows ratio plots in which all grid cells are included. For each ratio there are many points in the central U.S. where large values are seen in the ratio, yet the magnitude of the values are small. For example, when looking at a specific grid cell in eastern Montana, we see that the contribution percentage of that grid cell is approximately 273 times larger than the mortality percentage. However, if we look at the corresponding contribution we see that emissions in that grid cell contribute 0.003 mortalities per year. Also, the grid cell has a mortality value of only 0.0013 per year. It is evident that, while Figure 10c shows this grid cell as having a major importance on a ratio basis, the magnitudes of the contribution and mortalities show that the results in this cell are insignificant when compared to other cells. Therefore, we chose to only show a subset of the data.

When comparing the results in Figure 11 to contribution data for anthropogenic and biomass burning emissions combined, we are able to estimate that anthropogenic emissions of BC account for approximately 96.78% of mortalities associated with exposure to BC (12,177 mortalities). While this number is high, it is important to remember that a majority of mortalities attributed to exposure to BC occur in or near highly-populated locations. Many biomass burning events occur in areas in which there is a lower population, as the highly-populated urban areas tend to not have sufficient biomass to allow for large biomass burning contribution. From this figure, we see the largest contribution percentages occurring in densely-populated areas such as New York City, Los Angeles, Chicago, etc.

Figure 12 shows the ratio of gridded annual mortality percentage over gridded anthropogenic emission percentages on a log scale. The grid cells shaded yellow or red have a mortality percentage that is larger than the corresponding anthropogenic emission percentage, while cells shaded green or blue have a larger anthropogenic emission percentage than mortality percentage. From the view of the full domain (Figure 12a), we can see that the highly-populated urban areas have much larger mortality percentages than anthropogenic emission percentages. Figure 12c shows that grid cells along many of the interstates have larger anthropogenic emission percentages than mortality percentages. This is to be expected as transportation emissions account for a majority of anthropogenic U.S. BC emissions (approximately 80.8%, Sasser et al., 2011), and one would not expect many mortalities attributed to BC exposure to occur while on an interstate.

However, Figure 12b shows a few locations along California highway 99 in which there are larger mortality percentages than anthropogenic emission percentages. These grid cells

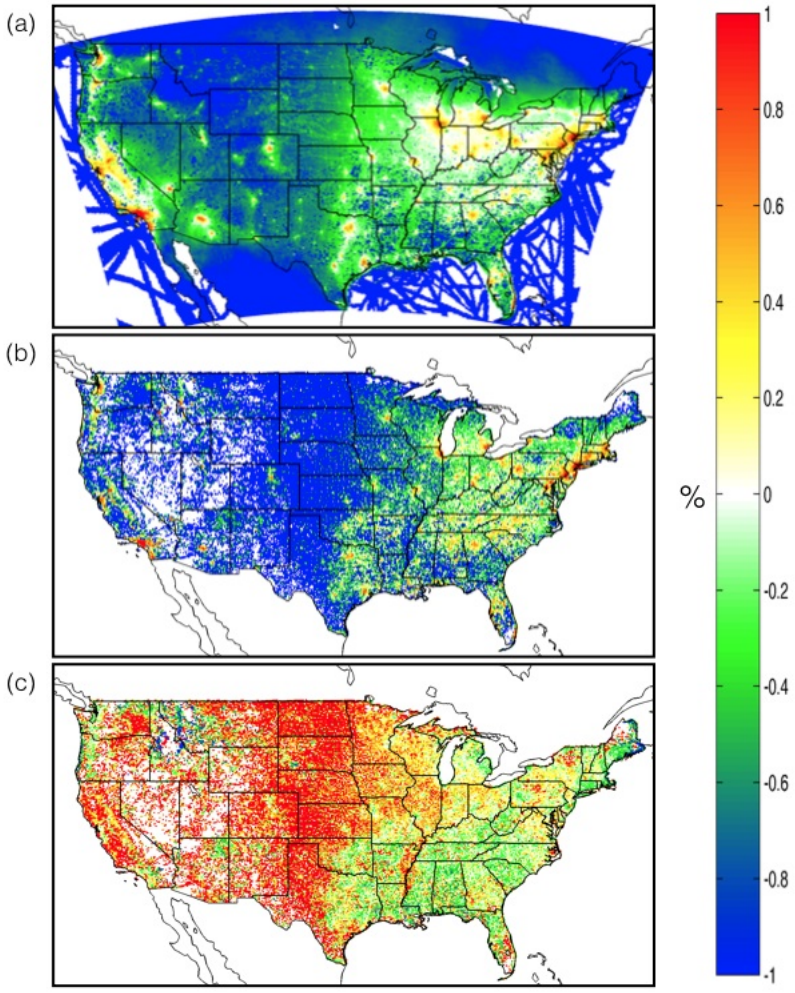

Figure 10: Ratio of (a) contribution percentage over emission percentage, (b) mortality percentage over emission percentage, and (c) contribution percentage over mortality percentage for every grid cell on a log scale.

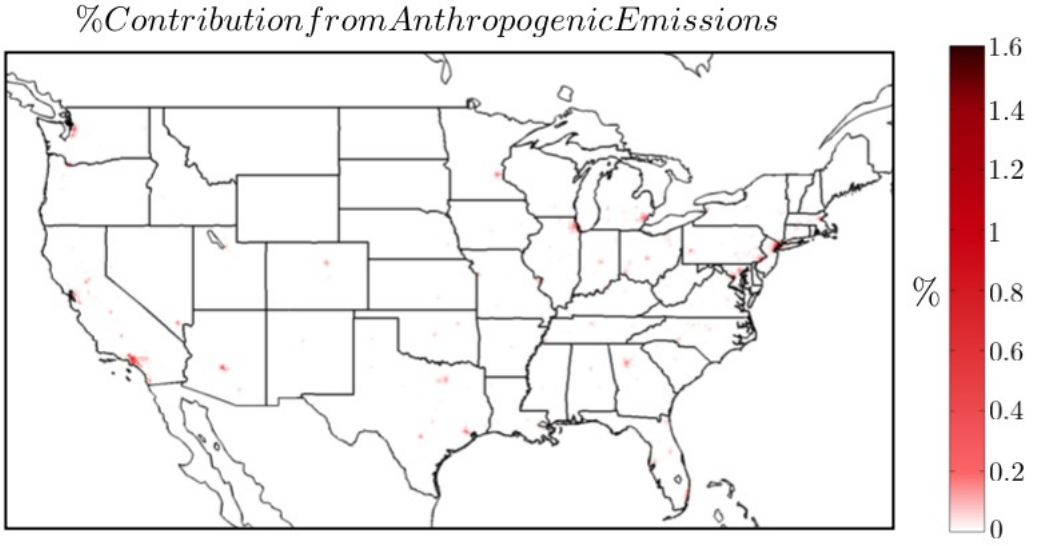

Figure 11: Contribution percentage from anthropogenic emissions.

correspond to cities in which the highway runs through (Fresno, Modesto, etc.). One would expect higher mortality rates in areas with large populations along highly-trafficked roadways.

For short-lived species like BC, one might expect emissions and contribution to be nearly equal throughout the model domain, as was the case for some of the studies in section 3.5, which assumed fixed damages throughout the domain. In order to evaluate this, we have analyzed the ratio of contribution percentage over anthropogenic emission percentage (Figure 13). By examining the ratio of contribution percentage to anthropogenic emission percentage, one can predict locations where BC emission controls would have the greatest benefit. The grid cells shaded red or yellow correspond to larger contribution percentages than anthropogenic emission percentages. Cells shaded green or blue have larger anthropogenic emission percentages than contribution percentages. It should be mentioned, however, that the contribution and emission percentages are percentages of the total contribution and emission, not percent of anthropogenic contribution and emission.

From the full domain (Figure 13a), we can again see that highly-populated urban areas tend to have much larger contribution percentages than anthropogenic emission percentages. From both Figures 13b and 13c, it is apparent that, while faint in Figure 13c, many major roadways have larger anthropogenic emission percentages than contribution percentages.

By comparing contribution percentages to anthropogenic emission percentages, it can be determined which emissions have the largest impact on human health. The fact that major roadways have higher emission percentages than contribution percentages suggests that, on a per unit emission basis, additional restrictions on vehicle emissions would not be the most efficient means to reducing national mortality attributed to exposure to BC. However, from the current analysis we cannot determine the percentage of contribution in major cities that comes from vehicle emissions. Distinguishing emissions by sector is an ongoing activity.

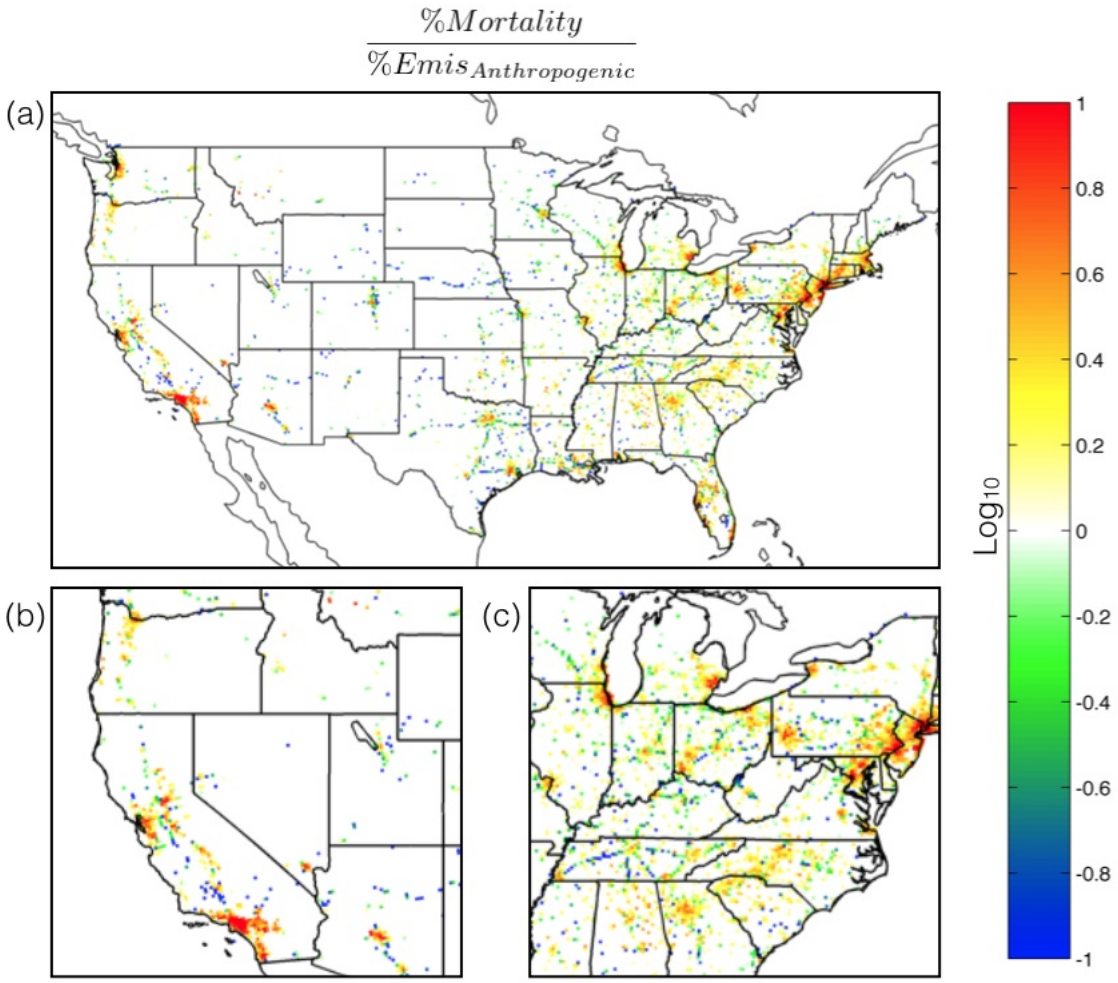

Figure 12: Ratio of gridded mortality percentage over gridded anthropogenic emission percentage, plotted on a log scale

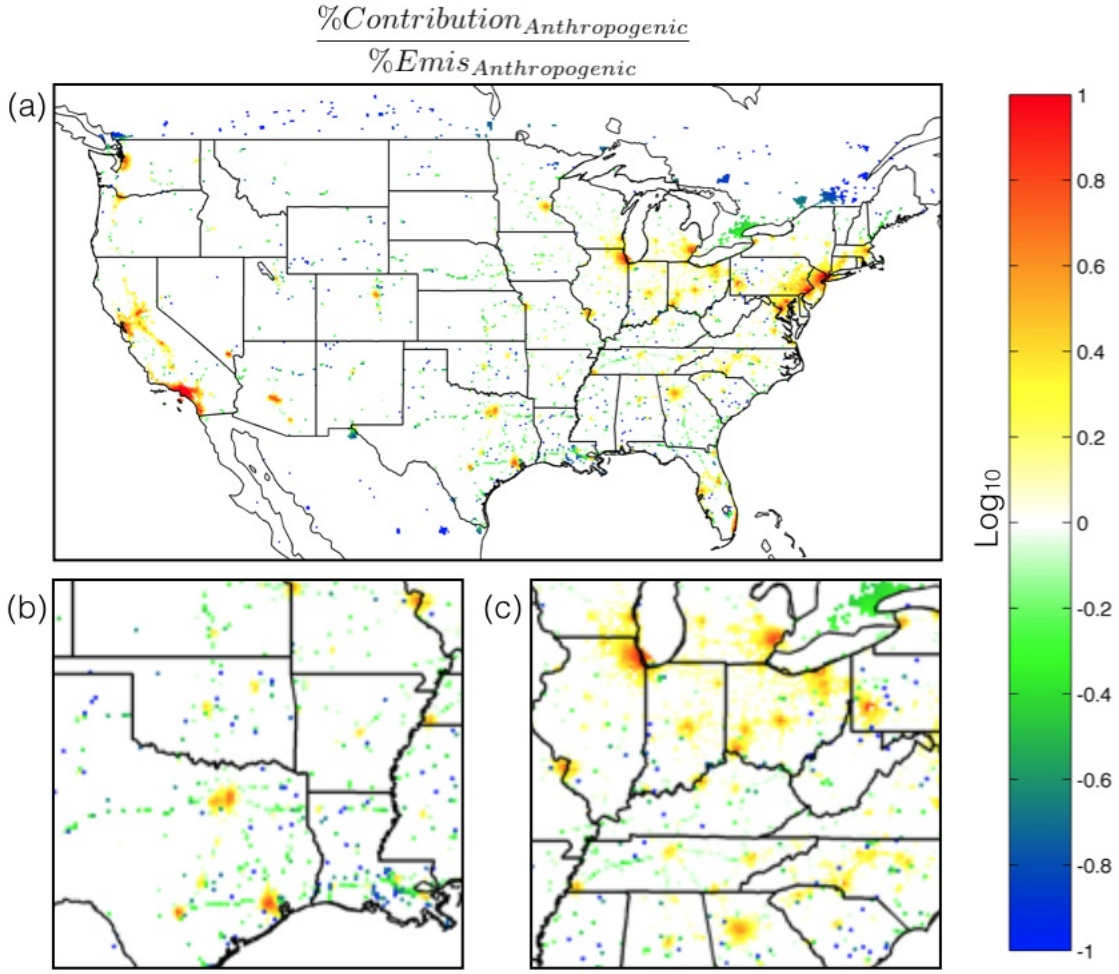

Figure 13: Ratio of gridded contribution percentage from anthropogenic emissions over gridded anthropogenic emission percentage, plotted on a log scale

As one might expect due to BC being a short-lived species that mortalities attributed to exposure to BC might be reduced most efficiently through reductions to emissions in highly populated areas. Through our adjoint sensitivity analysis, we are able to quantitatively separate the roles of emissions location and population distributions from atmospheric transport. To visualize this, we analyze the ratio of gridded contribution percentage over gridded mortality percentage (Figure 14). Grid cells shaded red or yellow correspond to locations that in a sense export death, while cells shaded green or blue correspond to locations that import death. From the plot of the full domain (Figure 14a), we can see that many of the major roadways have contribution percentages greater than mortality percentages. However, along some major roadways (such as Interstate-90), we see larger mortality percentages than contribution percentages.

Figure 14c shows that areas downwind of major emission locations (Connecticut, Rhode Island, eastern Massachusetts) have a higher percentage of mortality than contribution. Ad-

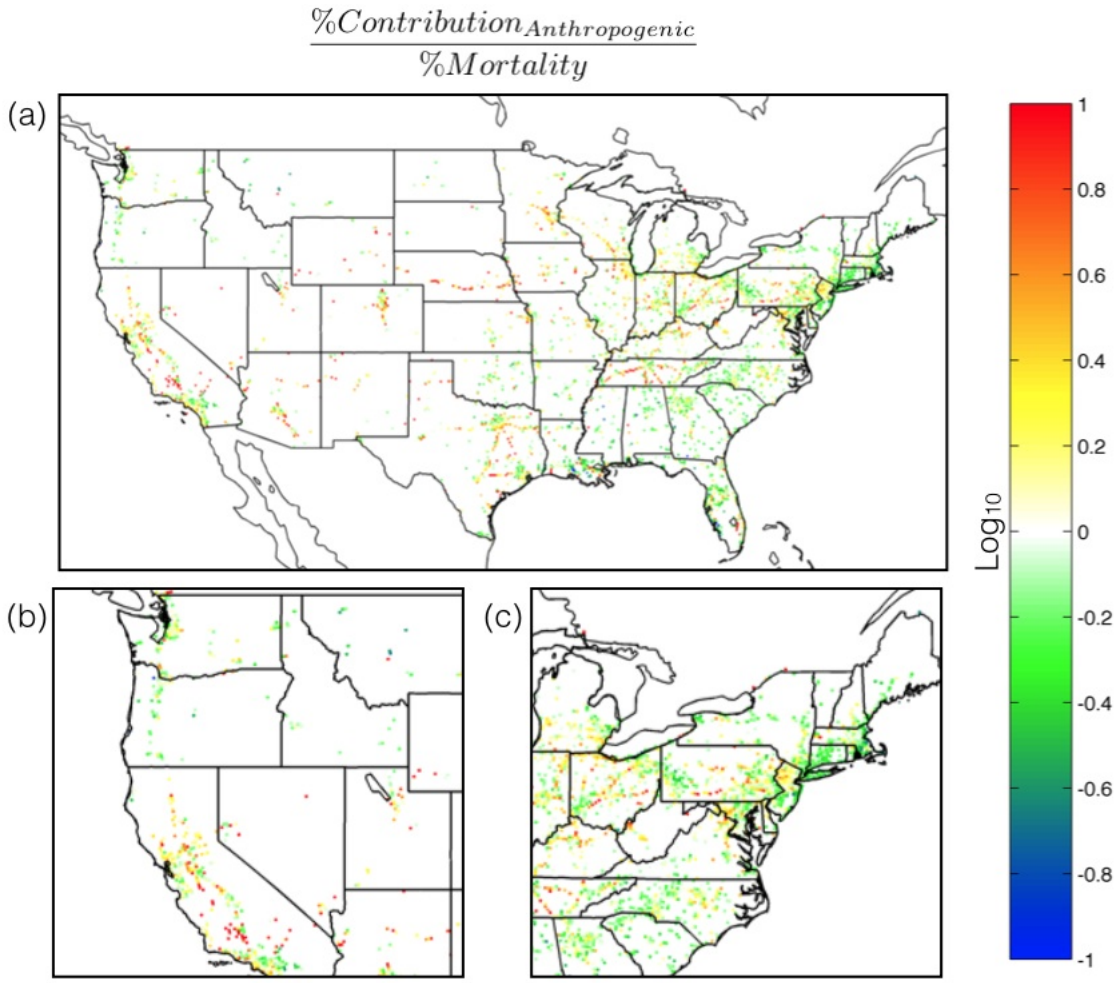

Figure 14: Ratio of gridded contribution percentage from anthropogenic emissions over gridded mortality percentage, plotted on a log scale

ditionally, many of the areas with higher contribution percentage than mortality percentage are upwind of majorly populated areas (northern New Jersey, west-southwest of New York City). The trend of larger contribution percentages than mortality percentages along major roadways is not limited to the northeastern U.S. In Figure 14b, we see many points along Interstate-5 that have substantially larger contribution percentages than mortality percentages. As with the northeastern U.S, Figure 14b shows higher mortality percentages downwind of high emission areas.

To further quantify the importance of including transport in health impact analyses of short-lived species, we compared mortality and contribution percentages to population percentages statistically in Figure 15. As one might expect, contribution is strongly correlated with population (Figure 15a). However, with a correlation coefficient of approximately 0.79, it is apparent that transport cannot be neglected when performing a source-attribution study on short-lived species. Mortalities are also highly correlated with population (Figure 15e),

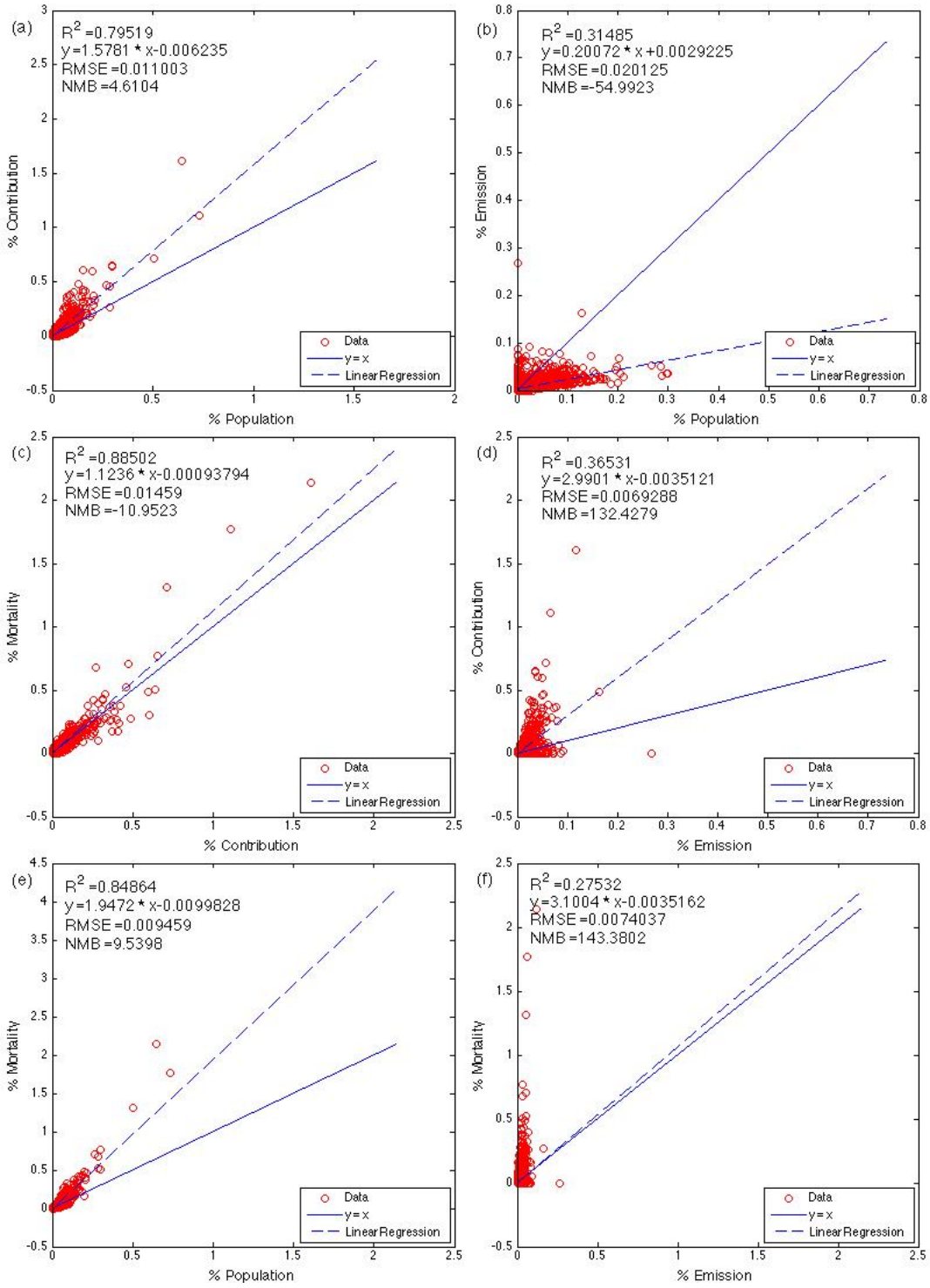

Figure 15: Comparison of (a) contribution percentage from anthropogenic emissions to population percentage, (b) anthropogenic emission percentage to population percentage, (c) mortality percentage to contribution percentage from anthropogenic emissions, (d) contribution percentage from anthropogenic emissions to anthropogenic emission percentage, (e) mortality percentage to population percentage, and (f) mortality percentage to anthropogenic emission percentage.

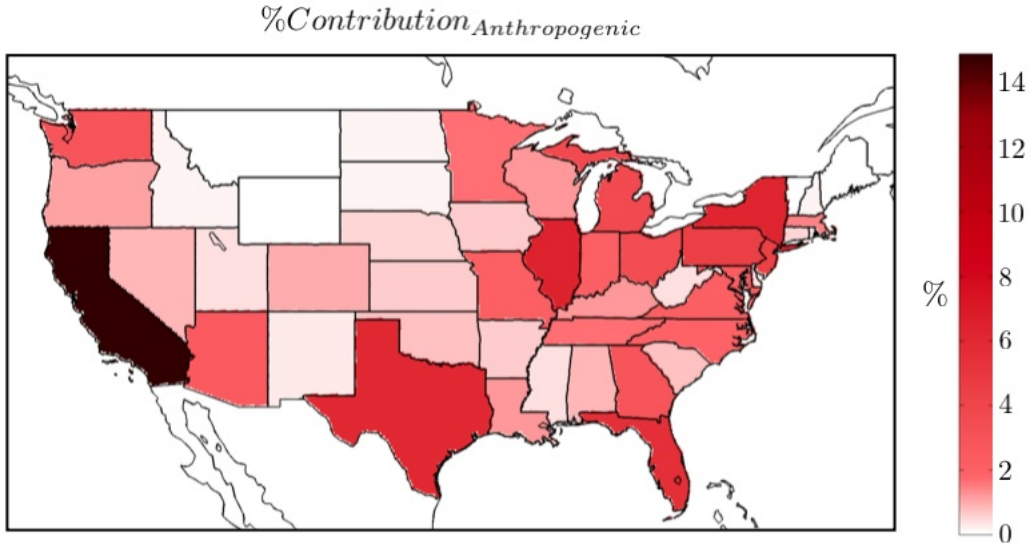

Figure 16: Contribution percentage from anthropogenic emissions, on a per state basis.

with a correlation coefficient of approximately 0.84. However, the slope of the bestfit line is nearly 2. As one might expect, mortalities are highly correlated with contribution (Figure 15c), with a correlation coefficient of approximately 0.88. It might be expected that emissions would be highly correlated with population (Figure 15b), however our analysis shows a correlation coefficient of only 0.31. When comparing anthropogenic emissions with contribution (Figure 15d) and mortality (Figure 15f), we obtain R^2 values of 0.36 and 0.27, respectively. Figure 15d shows that the locations with the highest anthropogenic emissions do not necessarily correspond to the highest contribution values. In fact, the largest anthropogenic emission plotted (0.266%) has a corresponding contribution percentage of 0.0008%. The regression of mortality on emission (Figure 15f) shows that a majority of high mortality percentages occur at locations that have low emission percentages. It is interesting to consider the most effective strategy for reducing health impacts if the highly spatially resolved analysis of this work was not available. In this case, the most effective controls strategies would apply stricter controls in locations with the highest mortalities, rather than locations with the highest emissions.

6.5.2 Sensitivity of BC Health Effects to Anthropogenic Emissions, Summed by State

In addition to sensitivity analyses on a gridded basis, we also analyzed and plotted the data on a per state basis. This kind of analysis is useful for policy decisions at the national level. For the plots on a per state basis, all grid cells were included. Also, a difference analysis (as opposed to the previous ratio analysis) was performed. This is due to the fact that, when summing the results over the states, the values in every state tend to be of the same order of magnitude.

Figure 16 shows the contribution percentage from anthropogenic emissions for 2007 on

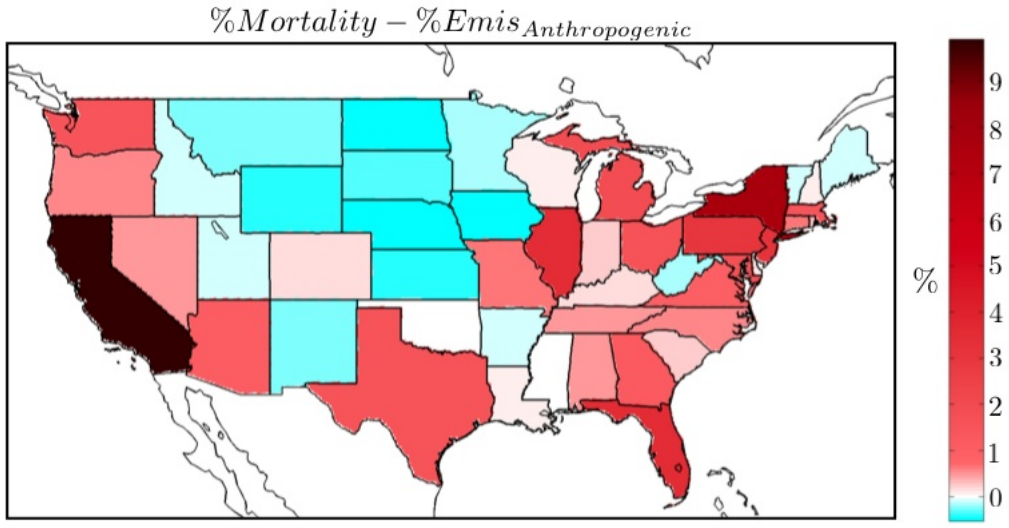

Figure 17: Mortality percentage minus anthropogenic emission percentage, on a per state basis.

a per state basis. The figure shows that a majority of annual mortalities attributed to exposure to BC are attributed to emissions from California (with approximately 14.9%, or 1,874 mortalities), followed by Illinois (with approximately 6.3%, or 792 mortalities), New York (with approximately 6.2%, or 780 mortalities) and Texas (with approximately 5.95%, or 749 mortalities).

While Figure 16 provides valuable information, it is beneficial to further analyze the data in an effort to see which states' emissions are contributing to more than their share of mortalities (when compared to emissions and mortalities), following Hakami et al. (2006). In this figure, states that are shaded red have higher mortality percentages than anthropogenic emission percentages. States that are shaded blue have higher anthropogenic emission percentages than mortality percentages. From Figure 17 we see that California and New York have the largest values, with 9.9% and 7.7%, respectively. Also, there are many states that have higher anthropogenic emission percentages than mortality percentages. However, while the maximum difference is 9.9% (California), the maximum difference that contains higher anthropogenic emission percentage is 0.53%. It should be noted that the mortality percentages in this figure sum to 100%, while the emission percentages sum to 60.9%. This is due to the fact that emission percentages are calculated from total emissions, and anthropogenic emissions of BC account for only 60.9% of total BC emissions for 2007.

In addition to comparing mortality percentages to anthropogenic emission percentages, we again compare contribution percentages to anthropogenic emission percentages (Figure 18). The results in this figure are similar to those in Figure 17, with a few differences. New York has a lower value (7.7% in Figure 17, 4.6% in Figure 18), while California has a higher value (9.9% in Figure 17, 11.55% in Figure 18). This figure suggests that emission reductions in California would have the largest impact, on a per unit emission basis, on

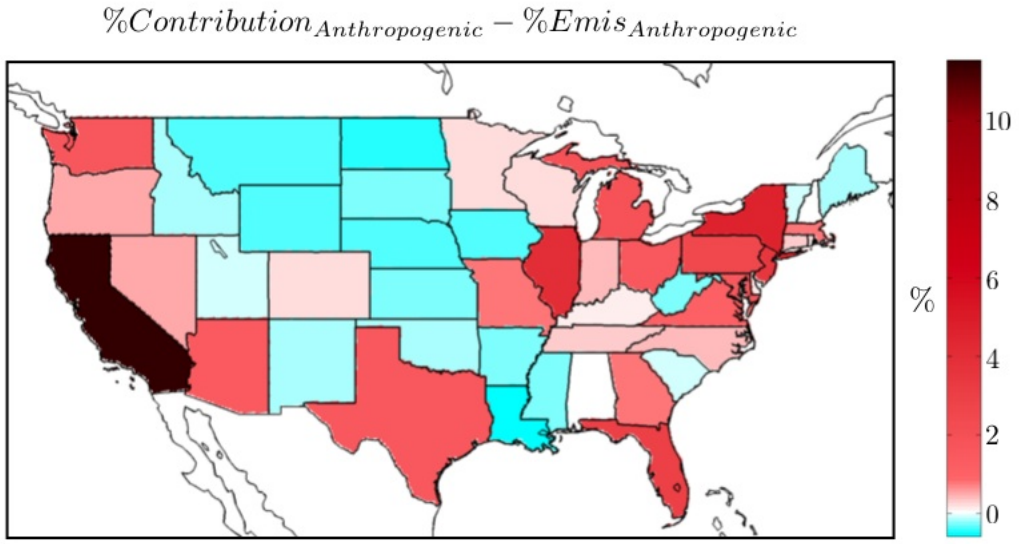

Figure 18: Contribution percentage from anthropogenic emissions minus anthropogenic emission percentage, on a per state basis.

reducing mortalities attributed to exposure to BC. As in Figure 17, there are many states with a higher anthropogenic emission percentage than contribution percentage. However, the maximum difference where anthropogenic emission percentage is larger than contribution percentage is 0.53%.

Figures 17 and 18 provide an estimate of which states have larger mortality and contribution percentages than emission percentages. However, it is beneficial to analyze the differences between contribution and mortality percentages for each state (Figure 19). States that are shaded yellow or red have higher contribution percentages than mortality percentages, while states shaded blue or green have higher mortality percentages than contribution percentages. This type of analysis allows us to estimate which states contribute disproportionally to the national health burden (red) and which would benefit the most from national-scale emissions reductions (blue).

With the exception of a few states (New Jersey, Illinois), a majority of the states east of the Mississippi have higher mortality percentages than contribution percentages, while a majority of states west of the Mississippi have higher contribution percentages than mortality percentages. This suggests that, even for short-lived species, transport processes must be included in order to obtain accurate estimates of contribution.

New York stands out as the state with the largest difference where mortality percentage is higher than contribution percentage, with a difference of 3.08%. Alternatively, California has the largest difference where contribution percentage from anthropogenic emissions is higher than mortality percentage, with a difference of 1.65%. This tells us that emissions originating in California contribute to more mortalities than there are mortalities in said state. Yet, there are more mortalities attributed to exposure to BC in New York than can be accounted for by BC emissions in New York.

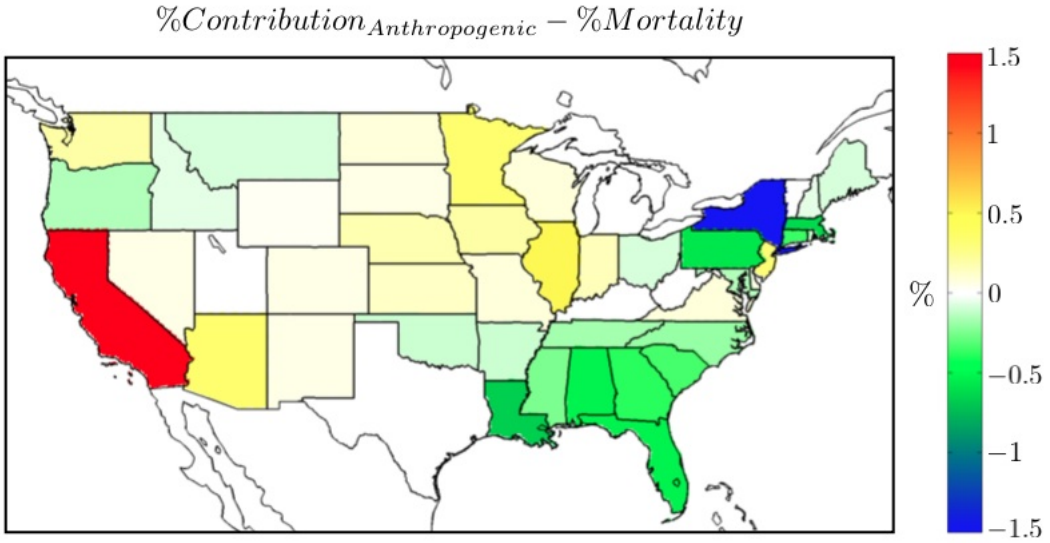

Figure 19: Contribution percentage from anthropogenic emissions minus mortality percentage, on a per state basis.

6.5.3 Sensitivity of BC Health Effects to Biomass Burning Emissions

In addition to analyzing the impact of anthropogenic emissions (Section 6.5.1), it is also important to analyze the impact of biomass burning emissions. Again, the ratio plots in this section include only a subset of grid cells in order to emphasize locations with the largest mortalities, emissions, and contributions. Figure 20 shows the gridded contribution percentage from biomass burning emissions. When comparing the data in this figure to Figure 9, we are able to estimate that biomass burning emissions of BC account for approximately 3.22% of mortalities associated with exposure to BC (406 mortalities).

As in section 6.5.1, we have analyzed the ratio of percent contribution from biomass burning to biomass burning emissions on a log scale (Figure 21). Grid cells shaded red and yellow have higher contribution percentage than biomass burning emission percentage, while cells shaded green and blue have higher biomass burning emission percentage than contribution percentage. One thing to note in this figure is that there are very few grid cells with a positive ratio. For this relationship, the lack of positive values is caused by the fact that the locations with highest contribution percentage from biomass burning still have very small contribution percentages (biomass burning contribution totals 3.22%, and the largest contribution value is 0.033%). While the location of highest contribution from biomass burning has a contribution value of 0.033%, the same grid cell has a biomass burning emission percentage of 0.2%.

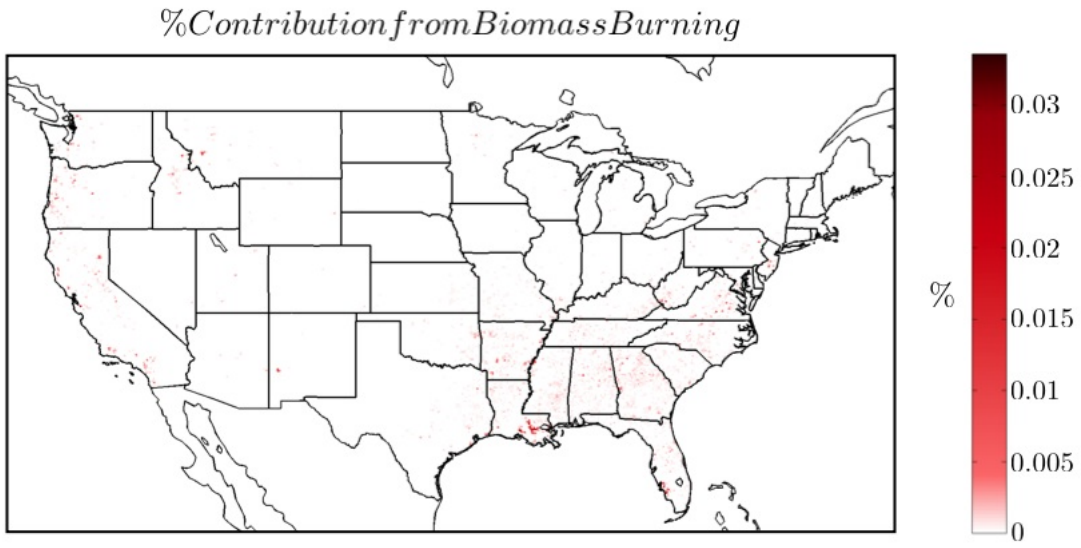

Figure 20: Contribution percentage from biomass burning emissions.

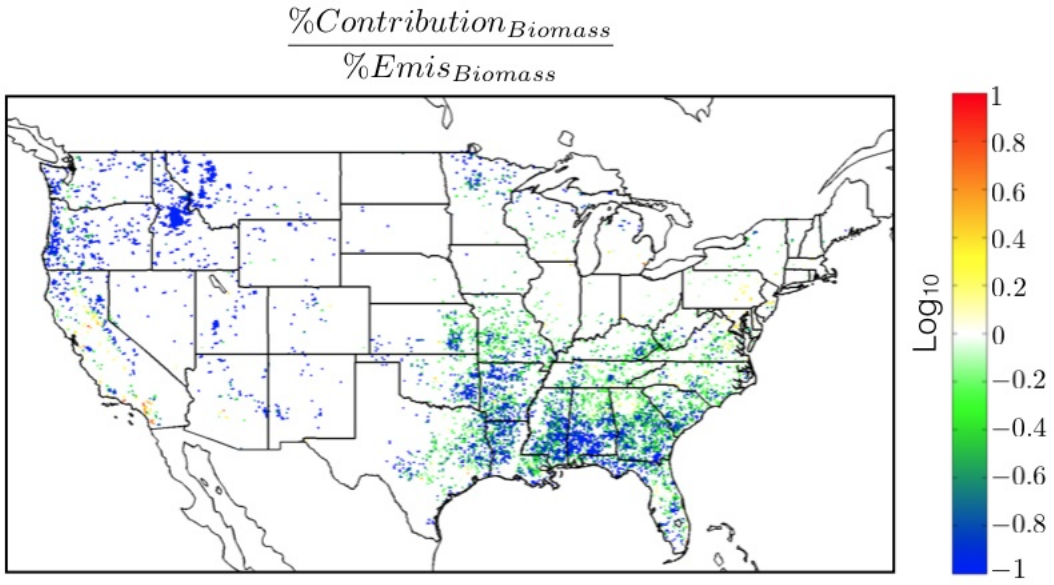

Figure 21: Ratio of gridded contribution percentage from biomass burning emissions over gridded biomass burning emission percentage, plotted on a log scale

7 Conclusions and Future Work

7.1 Conclusions

We have developed and validated the adjoint of the CMAQ air quality model for all processes except aqueous chemistry and gas phase chemistry. The model has been shown to accurately calculate BC sensitivities for all processes, and the aerosol adjoint model has been shown to validate for an array of species relationships. While further validation needs to be performed, we have shown the model to be sufficiently validated for studies focusing on BC.

We used the CMAQ adjoint model in order to estimate sensitivities of mortality attributed to exposure to BC with respect to emissions at a highly resolved spatial and sectoral level of specificity. While a majority of mortalities occur in highly-populated, urban locations, we were able to show that transport from less-populated regions plays an important role. Population density was shown to strongly correlate with mortality distributions, with a correlation coefficient of 0.845. However, the correlation between contribution and population resulted in a correlation coefficient of 0.79. This makes it apparent that transport cannot be neglected when performing source-attribution studies on short-lived species. We also determined that additional regulations to the highest emission locations would not be the most effective means of reducing mortalities attributed to BC exposure. Many of the highest contribution locations do not correspond to high emission percentages.

We calculated that, of the 12,583 mortalities attributed to exposure to BC in 2007, 12,177 of those were caused by anthropogenic emissions of BC. We were able to show that areas upwind of highly populated areas have much higher contribution percentages from anthropogenic emissions than mortality percentages. Also, many of the major interstates throughout the U.S. were shown to have substantially higher contribution percentages than mortality percentages, as one might expect. However, there are some major roadways (specifically I-90 in New York, and CA state route 99) that have higher mortality percentages than contribution percentages. This is most likely attributed to the high population areas in which the roadways pass through. Additionally, we were able to show that many of the major roadways have larger emission percentages than contribution percentages. This suggests that while the transportation sector is responsible for 52.3% of total BC emissions in the U.S., controlling those emissions may not be the most optimal strategy to reduce mortalities on a per unit emission basis. On the other hand, biomass burning emissions of BC, which account for approximately 35.3% of total BC emissions in the U.S., account for only 406 mortalities per year.

7.2 Future Work

Adjoint Development While section 5.1 showed that the aerosol module currently validates for most species relationships, it is apparent that further validation tests need to be performed in order to analyze the remaining discrepancies between the adjoint and FD or CVM sensitivities for specific relationships. Additionally, more robust testing needs to be performed for the model as a whole. Section 5.2 presented some preliminary results validating one specific configuration of the adjoint, yet the full adjoint model will need to be

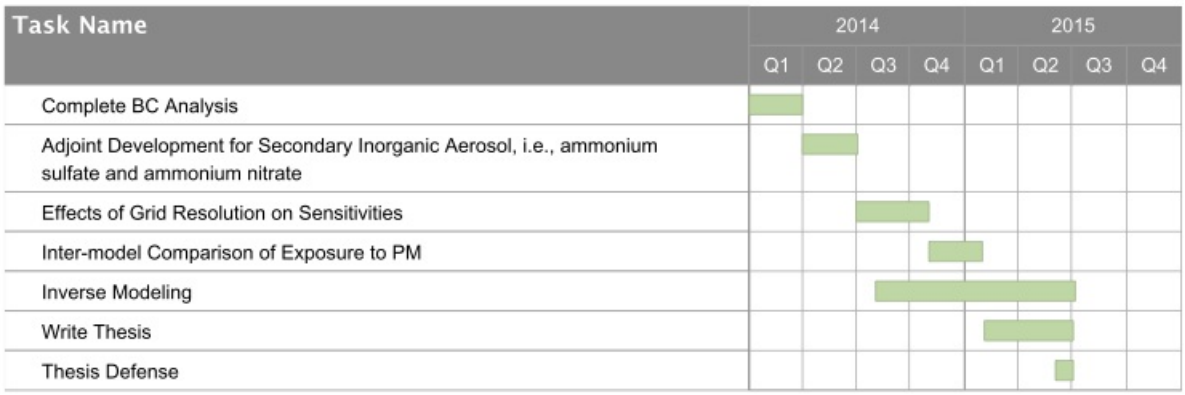

Figure 22: Timeline for Future Work

validated as a whole. This involves the inclusion of aqueous chemistry, and gas-phase chemistry in the model, as well as horizontal transport. This will take place over the summer, after the current BC health impact analysis is complete.

Inverse Modeling We will be collaborating with a group from Atmospheric and Environmental Research Inc. to investigate the sources, formation, and direct radiative impacts of *ammonium nitrate* and *ammonium sulfate* aerosols. There are large uncertainties in ammonia precursor emissions, which result in large uncertainties in the vertical distribution, and radiative impacts of the ammonium sulfate and ammonium nitrate aerosol. Using measurements from the CalNex field campaign, and satellite retrievals from the TES instrument aboard NASA's Aura satellite, these uncertainties will be reduced through inverse modeling with the CMAQ adjoint model. Upon obtaining constrained ammonia emissions, the CMAQ model will be used in conjunction with the RRTM radiation code developed at AER to estimate the regional radiative and air quality impacts of these aerosols.

Effects of Grid Resolution on Sensitivities Studies have shown that model resolution can have a substantial effect on the estimation of exposure to PM (Punger and West, 2013). Yet, few studies have been performed to show the effect of grid resolution on the marginal sensitivities of human pollutant exposure to emissions.. We plan to further our analysis of the health impacts of BC emissions by quantifying the effect that grid resolution (12-km grid and 36-km grid) has on source-receptor interactions. This will take place over the fall semester of 2014, after the adjoint is fully validated and includes secondary inorganic aerosols.

Inter-Model Comparison of Exposure to PM While this project has focused on estimating the effects of gridded emissions on national mortality attributed to BC exposure using the CMAQ adjoint model, similar studies can be performed with other chemical transport models that have an adjoint developed. We plan to perform similar calculations using the GEOS-Chem adjoint, and will compare the results from the two models. In addition to the comparison of sensitivities from the two adjoint models, we will also be comparing the estimated mortalities obtained from forward model simulations. This will take from the end

of the fall 2014 semester to the beginning of the spring 2015 semester, after the effects of grid resolution have been analyzed.

References

Environmental Benefits and Mapping Program (BenMAP, Version 4.0.67). Abt Associates, Inc., 2013. Bethesda, MD.

M Amann, Richard Derwent, B Forsberg, F Hurley, M Krzyznowski, B Kuna-Dibber, S Larssen, F de Leeuw, S Liu, J Schneider, P Schwarze, D Simposon, J Stedman, P Straehl, L Tarrason, and L van Bree. Health Risks of Particulate Matter from Long-range Transboundary Air Pollution. World Health Organization, 2006.

Susan C Anenberg, Larry W Horowitz, Daniel Q Tong, and J Jason West. An Estimate of the Global Burden of Anthropogenic Ozone and Fine Particulate Matter on Premature Human Mortality Using Atmospheric Modeling. *Environmental Health Perspectives*, 118 (9):1189–1195, April 2010.

K W Appel, C Chemel, S J Roselle, and X V Francis. Examination of the Community Multiscale Air Quality (CMAQ) model performance over the North American and European domains. *Atmospheric Environment*, 2012.

KW Appel, AB Gilliland, G Sarwar, and RC Gilliam. Evaluation of the Community Multiscale Air Quality (CMAQ) Model Version 4.5: Sensitivities Impacting Model Performance Part I - Ozone. *Atmospheric Environment*, 41(40):9603–9615, 2007.

KW Appel, PV Bhave, AB Gilliland, G Sarwar, and SJ Roselle. Evaluation of the community multiscale air quality (CMAQ) model version 4.5: Sensitivities impacting model performance; Part II—particulate matter. *Atmospheric Environment*, 42(24):6057–6066, August 2008.

W Baur and V Strassen. The Complexity of Partial Derivatives. *Theoretical Computer Science*, 22(3):317–330, 1983.

M L Bell, K Ebisu, R D Peng, J M Samet, and F Dominici. Hospital Admissions and Chemical Composition of Fine Particle Air Pollution. *American Journal Of Respiratory And Critical Care Medicine*, 179(12):1115–1120, June 2009.

FS Binkowski and SJ Roselle. Models-3 community multiscale air quality (CMAQ) model aerosol component - 1. Model description. *Journal of Geophysical Research-Atmospheres*, 108:–, 2003.

T C Bond, S J Doherty, D W Fahey, P M Forster, T Berntsen, B J DeAngelo, M G Flanner, S Ghan, B Kärcher, and D Koch. Bounding the role of black carbon in the climate system: A scientific assessment. *Journal of Geophysical Research-Atmospheres*, 2013.

O Boucher, D Randall, P Artaxo, C Bretherton, G Feingold, P Forster, V M Kerminen, Y Kondo, H Liao, U Lohmann, P Rasch, S K Satheesh, S Sherwood, B Stevens, and X Zhang. Clouds and Aerosols. *Climate Change 2013: The Physical Science Basis. Contribution of Working Group 1 to the Fifth Assessment Report of the Intergovernmental Panel on Climate Change*, pages 1–149, August 2013.

S L Capps, D K Henze, A Hakami, A G Russell, and A Nenes. ANISORROPIA: the adjoint of the aerosol thermodynamic model ISORROPIA. *Atmospheric Chemistry and Physics Discussion*, 11(8):23469–23511, 2011.

A J Cohen, H R Anderson, B Ostro, K D Pandey, M Krzyzanowski, N Kunzli, K Gutschmidt, A Pope, I Romieu, J M Samet, and K Smith. The global burden of disease due to outdoor air pollution. *Journal of Toxicology and Environmental Health-Part a-Current Issues*, 68 (13-14):1301–1307, 2005.

O Dubovik, T Lapyonok, Y J Kaufman, M Chin, P Ginoux, R A Kahn, and A Sinyuk. Retrieving global aerosol sources from satellites using inverse modeling. *Atmospheric Chemistry and Physics*, 8(2):209–250, 2008.

H Elbern, H Schmidt, O Talagrand, and A Ebel. 4D-Variational Data Assimilation with an Adjoint Air Quality Model for Emission Analysis. *Environmental Modelling & Software*, 15(6-7):539–548, 2000.

U S EPA. *Benefits and Costs of the Clean Air Act from 1990 To 2020*. Summary Report. US EPA, March 2011.

US EPA. Integrated Science Assessment for Particulate Matter (Final Report). *U.S. Environmental Protection Agency, Washington, DC*, pages 1–2228, February 2009.

N Fann, C M Fulcher, and B J Hubbell. The influence of location, source, and emission type in estimates of the human health benefits of reducing a ton of air pollution - Springer. *Air Quality*, 2009.

Neal Fann, Kirk R Baker, and Charles M Fulcher. Characterizing the pm2.5-related health benefits of emission reductions for 17 industrial, area and mobile emission sectors across the u.s. *Environment International*, 49(C):141–151, November 2012a.

Neal Fann, Amy D Lamson, Susan C Anenberg, Karen Wesson, David Risley, and Bryan J Hubbell. Estimating the National Public Health Burden Associated with Exposure to Ambient PM2.5 and Ozone. *Risk Analysis*, 32(1):81–95, January 2012b.

Mark G Flanner, Charles S Zender, James T Randerson, and Philip J Rasch. Present-day climate forcing and response from black carbon in snow. *Journal of Geophysical Research*, 112(D11), June 2007.

P Forster, V Ramaswamy, P Artaxo, T Berntsen, R Betts, D W Fahey, J Haywood, J Lean, D C Lowe, G Myhre, J Nganga, R Prinn, G B Raga, M Schulz, and R Van Dorland. *Changes in Atmospheric Constituents and in Radiative Forcing*. Climate Change 2007: The Physical Science Basis. Contribution of Working Group 1 to the Fourth Assessment Report of the Intergovernmental Panel on Climate Change. Cambridge University Press, Cambridge, United Kingdom and New York, NY, USA, September 2007.

C Fountoukis and A Nenes. ISORROPIA II: a computationally efficient thermodynamic equilibrium model for K+–Ca 2+–Mg 2+–NH 4+–Na+–SO 4 2–NO 3–Cl–H 2 O aerosols. *Atmospheric Chemistry and Physics*, 7(17):4639–4659, 2007.

Eric M Fujita, David E Campbell, Barbara Zielinska, Judith C Chow, Christian E Lindhjem, Allison DenBleyker, Gary A Bishop, Brent G Schuchmann, Donald H Stedman, and Douglas R Lawson. Comparison of the MOVES2010a, MOBILE6.2, and EMFAC2007 mobile source emission models with on-road traffic tunnel and remote sensing measurements. *Journal of the Air & Waste Management Association*, 62(10):1134–1149, October 2012.

R Giering and T Kaminski. Recipes for Adjoint Code Construction. *Acm Transactions On Mathematical Software*, 24(4):437–474, 1998.

Andreas Griewank. Achieving logarithmic growth of temporal and spatial complexity in reverse automatic differentiation. *Optimization Methods and software*, 1(1):35–54, 1992.

John H Seinfeld and Spyros N Pandis. Atmospheric Chemistry and Physics: From Air Pollution to Climate Change, (2nd Edition). *John Wiley & Sons, Inc.*, 2006.

A Hakami, DK Henze, JH Seinfeld, T Chai, Y Tang, GR Carmichael, and A Sandu. Adjoint Inverse Modeling of Black Carbon During the Asian Pacific Regional Aerosol Characterization Experiment. *Journal of Geophysical Research-Atmospheres*, 110(D14):D14301, 2005.

Amir Hakami, John H Seinfeld, Tianfeng Chai, Youhua Tang, Gregory R Carmichael, and Adrian Sandu. Adjoint Sensitivity Analysis of Ozone Nonattainment over the Continental United States. *Environmental Science & Technology*, 40(12):3855–3864, June 2006.

Amir Hakami, Daven K Henze, John H Seinfeld, Kumaresh Singh, Adrian Sandu, Soontae Kim, Daewon Byun, and Qinbin Li. The adjoint of CMAQ. *Environmental Science & Technology*, 41(22):7807–7817, 2007.

Shauna L Hallmark, Randall Guensler, and Ignatius Fomunung. Characterizing on-road variables that affect passenger vehicle modal operation. *Transportation Research Part D: Transport and Environment*, 7(2):81–98, 2002.

S Hanna, A G Russell, James Wilkinson, and J Vukovich. Review of BEIS3 Formulation and Consequences Relative to Air Quality Standards. *EPRI Tech. Report 1005159, EPRI, 3412 Hillview Ave., Palo Alto, CA 94304, 2002*, pages 1–170, May 2002.

Steven R Hanna and James Wilkinson. Analytical estimation of uncertainties in biogenic emissions calculated by BEIS3 due to uncertainties in model inputs and parameters. pages 8–10, 2004.

J Hansen. Efficacy of climate forcings. *Journal of Geophysical Research*, 110(D18):D18104, 2005.

J Hansen, M Sato, and R Ruedy. Radiative forcing and climate response. *Journal of Geophysical Research*, 102(D6):6831, March 1997.

D K Henze, A Hakami, and J H Seinfeld. Development of the adjoint of GEOS-Chem. *Atmospheric Chemistry and Physics*, 7(9):2413–2433, 2007.

D K Henze, J H Seinfeld, and D T Shindell. Inverse modeling and mapping US air quality influences of inorganic PM 2.5 precursor emissions using the adjoint of GEOS-Chem. *Atmospheric Chemistry and Physics*, 9(16):5877–5903, 2009.

DK Henze, JH Seinfeld, W Liao, A Sandu, and GR Carmichael. Inverse Modeling of Aerosol Dynamics: Condensational Growth. *Journal of Geophysical Research-Atmospheres*, 109 (D14):D14201, 2004.

N Huneeus, O Boucher, and F Chevallier. Simplified aerosol modeling for variational data assimilation. *Geoscientific Model Development*, 2(2):213–229, 2009.

Mark Z Jacobson. Control of fossil-fuel particulate black carbon and organic matter, possibly the most effective method of slowing global warming. *Journal of Geophysical Research*, 107(D19):4410, 2002.

Nicole A H Janssen, Gerard Hoek, Milena Simic-Lawson, Paul Fischer, Leendert van Bree, Harry ten Brink, Menno Keuken, Richard W Atkinson, H Ross Anderson, Bert Brunekreef, and Flemming R Cassee. Black carbon as an additional indicator of the adverse health effects of airborne particles compared with PM10 and PM2. 5. *Environmental Health Perspectives*, 119(12):1691–1699, August 2011.

Daniel Krewski, Michael Jerrett, Richard T Burnett, Renjun Ma, Edward Hughes, Yuanli Shi, Michelle C Turner, C Arden Pope, George Thurston, Eugenia E Calle, Michael J Thun, Bernie Beckerman, Pat DeLuca, Norm Finkelstein, Kaz Ito, D K Moore, K Bruce Newbold, Tim Ramsay, Zev Ross, Hwashin Shin, and Barbara Tempalski. Extended follow-up and spatial analysis of the American Cancer Society study linking particulate air pollution and mortality. *Research report (Health Effects Institute)*, (140):5–114– discussion 115–36, May 2009.

Johanna Lepeule, Francine Laden, Douglas Dockery, and Joel Schwartz. Chronic exposure to fine particles and mortality: an extended follow-up of the Harvard Six Cities study from 1974 to 2009. *Environmental Health Perspectives*, 120(7):965–970, July 2012.

PT Martien and RA Harley. Adjoint Sensitivity Analysis for a Three-Dimensional Photochemical Model: Implementation and Method Comparison. *Environmental Science & Technology*, 40(8):2663–2670, 2006.

MR Mebust, BK Eder, FS Binkowski, and SJ Roselle. Models-3 community multiscale air quality (CMAQ) model aerosol component - 2. Model evaluation. *Journal of Geophysical Research-Atmospheres*, 108:–, 2003.

N Z Muller and R Mendelsohn. Measuring the damages of air pollution in the United States. *Journal of Environmental Economics and ...*, 2007.

Nicholas Z Muller, Robert Mendelsohn, and William Nordhaus. Environmental Accounting for Pollution in the United States Economy. *American Economic Review*, 101(5):1649–1675, August 2011.

Robert Pincus and Marcia B Baker. Effect of precipitation on the albedo susceptibility of clouds in the marine boundary layer. *Nature*, 372(6503):250–252, November 1994.

Jonathan E Pleim. A Combined Local and Nonlocal Closure Model for the Atmospheric Boundary Layer. Part I: Model Description and Testing. *Journal Of Applied Meteorology And Climatology*, 46(9):1383–1395, September 2007.

CA Pope, RT Burnett, GD Thurston, MJ Thun, EE Calle, D Krewski, and JJ Godleski. Cardiovascular Mortality and Long-Term Exposure to Particulate Air Pollution - Epidemiological Evidence of General Pathophysiological Pathways of Disease. *Circulation*, 109(1): 71–77, 2004.

Elizabeth M Punger and J Jason West. The effect of grid resolution on estimates of the burden of ozone and fine particulate matter on premature mortality in the USA. *Air Quality, Atmosphere & Health*, 6(3):563–573, May 2013.

A Sandu, W Liao, GR Carmichael, DK Henze, and JH Seinfeld. Inverse Modeling of Aerosol Dynamics Using Adjoints: Theoretical and Numerical Considerations. *Aerosol Science And Technology*, 39(8):677–694, 2005.

E Sasser, J Hemby, K Adler, S Anenber, C Bailey, L Brockman, L Chappell, B DeAngelo, R Damberg, J Dawson, N Frank, M Geller, G Hagler, B Hemming, L Jantarasami, T Luben, J Mitchell, J Moss, V Rao, J Rice, M Sarofim, J Somers, C Spells, S Terry, and M Witosky. Report to Congress on Black Carbon. US EPA, 2011.

S Twomey. Pollution and Planetary Albedo. *Atmospheric Environment*, 8(12):1251–1256, 1974.